Development and Validation of a Turbulent Flame Propagation Model

Thesis for Master of Science by Simon Bjerkborn

Lund Combustion Engineering – LOGE AB
and
Physics Department – Lund University

Examiner:
Carl-Erik Magnusson, Physics Department, Lund University
Supervisors:
Cathleen Perlman, LOGE AB

Abstract

The aim of this thesis was to develop a model for flame propagation, to implement in a zero-dimensional engine simulation tool (DARS 0d-SRM) which previously only used fitted Wiebe-functions to describe the flame propagation. The idea was to create a model which could replace or complement the Wiebe function, but with predictive capabilities, avoiding the need to perform curve-fitting when certain parameters are changed.

In addition to selecting and developing a suitable mathematical model for calculating the turbulent flame propagation speed, the project also included developing a suitable model for calculating the flame volume for a given flame radius. To achieve maximum precision, a Monte Carlo model was created for this purpose.

The flame propagation model was validated against an earlier study, and against two sets of experimental data. Good correlation was found.

Nomenclature

Variables

Roman letters		
t	Time	s
l_L	Integral length scale	m
l_K	Kolmogorov length scale	m
u'	Turbulence intensity	m/s
h_c	Woschni heat transfer coeff.	W/m^2K
w	Average gas velocity	m/s
p	Pressure	Pa
T	Temperature	K
V	Volume	m^3
S	Speed	m/s
k	Kinetic energy	J
ν	Viscosity	m^2/s
a	Equation constant	
b	Equation constant	
d	Equation constant	
Greek letters		
τ	Turbulent mixing time	s
θ	Crank angle degree	^{o}
δ_L	Laminar flame thickness	m
ρ	Density	kg/m^3
Θ	Reduced temperature	
ϵ	Scalar dissipation rate	m^2/s^3
ω	Reaction rate	s^{-1}
Φ	Equivalence ratio	

Subscripts

T	Turbulent
L	Laminar

b	Burned
u	Unburned

Abbreviations

MFB	Mass Fraction Burned
SRM	Stochastic Reactor Model
SI	Spark Ignition
CAD	Crank Angle Degree
IEM	Interaction by Exchange with Mean
TFP	Turbulent Flame Propagation
RPM	Revolutions Per Minute
TDC	Top Dead Center
ATDC	After Top Dead Center
BTDC	Before Top Dead Center
CFD	Computational Fluid Dynamics

Contents

1. Introduction

The two-zone stochastic reactor model (SRM) has been proven to be a comparatively quick and effective way to simulate SI engines to predict engine knock and emissions [1]. Being zero-dimensional however limits the predictive capabilities of the model, since many observable phenomena in the engine are only possible to model predictably with a spatial resolution, such as the process of flame propagation and combustion speed.

This work aims to replace or complement the deterministic Wiebe model with a predictive flame propagating model. By using a laminar flame speed library combined with an analytically derived model for turbulent flame speed and Monte Carlo geometry calculations, the calculation time advantage of having a zero-dimensional model is maintained while one is also able to predict effects of cylinder geometry and turbulence on the flame propagation.

Chapter 1 will provide an introduction of the SRM model and the outline of the work performed in this thesis, chapters 2-4 will discuss the choice and development of the flame propagation model created in this thesis, including the turbulence modelling and the Monte Carlo geometry solution, as well as a discussion of the wall quenching phenomenon and how it could be included in the model. Chapter 6 contains a short study of the sensitivity in the varying input parameters of the model and a validation against a previous study and two sets of experimental data.

1.1 The SI engine

The most general description of the spark ignition (SI) engine is fuel, generally premixed with air, being compressed by a piston in a cylinder and ignited by a spark plug. The combustion takes place locally in a flame which propagates through the cylinder, and the increase in pressure then causes the piston to be pushed down again. The exhaust gas is

extracted from the cylinder, new gas is injected and the cycle restarts.

1.2 The 0-d SRM model

Although the flame propagation model created could be applied to most engine simulation tools using the Wiebe function (see Ch. 1.2.3) to describe the burning progress, the particular tool used in the development of the flame propagation model is a zero dimensional two-zone stochastic reactor model. The mass of the cylinder gas is divided into two separate zones, burned and unburned, and the mass of each zone is divided into a number of particles. The particles, however, carry no spatial information and are merely a discretization of the mass. The distribution of the state variables is described using a probability density function. In each time step, a new probability density function is calculated by numerically solving its transport equation. Processes in the cylinder are modelled one by one in an operator splitting loop according to Fig. 1. In the cases presented in this work, time steps of 0.5 crank angle degrees (CAD) were used. For a decreased calculation time, the model can be run with time steps over 1 CAD, though it might result in small systematic errors, mainly stemming from interpolation.

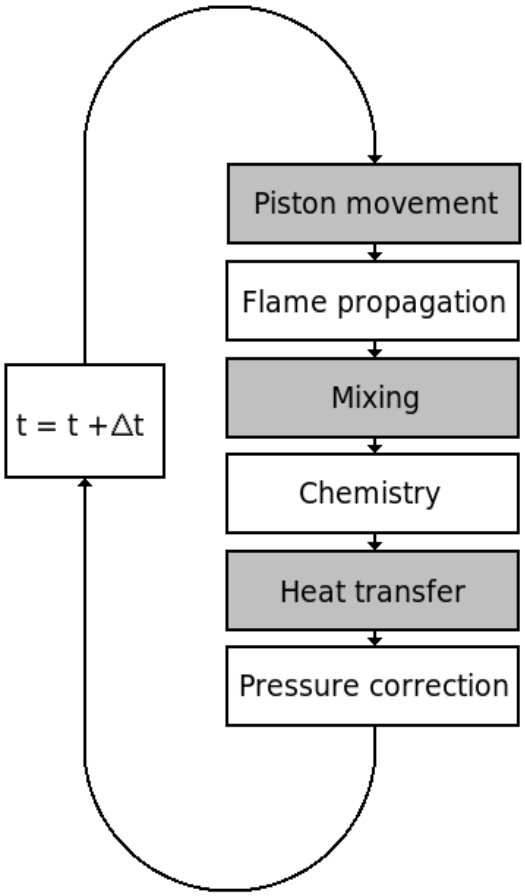

Fig. 1 – The operator splitting loop for the SI-SRM

The heat transfer step and the mixing are of particular relevance to the flame propagation model, and will be discussed in general terms below. For a more detailed description on the implementation of the models, see for example [1] and [2].

1.2.1 Mixing

Initial fluctuations in the enthalpy between particles need to be smoothed out over time, and the lack of a spatial resolution makes it impossible to have a purely phenomenologically based mixing model. The SRM code includes two approaches; the IEM (Ch. 1.2.1a) and the curl (Ch. 1.2.1b) model. During the development of this model, the curl model was used.

The pace of the mixing is decided by the turbulent mixing time τ, defined according to Eq. 1, with l_L being the integral length scale, a measurement of the scale of the largest turbulence eddies, and u' being
the turbulent root-mean-square (RMS) velocity of the gas.

$$\tau = \frac{l_L}{u'} \quad (1)$$

1.2.1a The IEM mixing model

The Interaction by Exchange with the Mean (IEM) model moves the value of each particle towards the mean of the corresponding value for all particles. This is coherent with the expected end results (in a final homogenous state, the global temperature should be the mass-weighted mean of the initial temperature, save for a flux of energy due to heat loss or chemical reactions) and with the preservation of enthalpy through the mixing process. However, it does not provide a very accurate description of the process under way. Since the SRM code is used to predict autoignition based on local state variables of the gas, a realistic model of the stochastic fluctuations in the gas is needed.

1.2.1b The Curl mixing model

Unlike the IEM model, the Curl mixing model randomly selects pairs of particles and assigns them their mutual weighted average values. As for the IEM, the average properties of the gas remain unchanged throughout the mixing but with a large enough number of particles it also provides a comparatively realistic image of the mixing of a gas. The lack of spatial resolution still leaves some behaviour unmodelled, such as a systematic non-homogeneous temperature field in the cylinder gas.

1.2.2 Heat transfer

The transfer of heat energy between the gas and the cylinder walls is calculated using a

simplification of Woschni's semi-empirical heat transfer correlation, according to Eq. 2

$$h_c = 3.26\, B^{0.2}\, p^{0.8}\, w^{0.8}\, T^{-0.55} \quad (2)$$

where h_c is the heat transfer coefficient, measured in W/m^{2}K and w is the average cylinder gas velocity, calculated according to Eq. 3:

$$w = C_1 \bar{S}_p + C_2 \frac{V_d T_r}{p_r V_r}(p - p_m) \quad (3)$$

In Eq. 2 the cylinder bore (the diameter of the cylinder) is B and T is the mean cylinder gas temperature. In Eq. 3 C_1 and C_2 are constants, V_d is the displaced volume, p_r, V_r and T_r are the pressure, volume and temperature at inlet valve closing, and p_m is the motored pressure. $\bar{S}_p$ is the mean piston speed.

Using this together with an approximation of the cylinder wall area, an enthalpy flux can be calculated. This enthalpy is then in each time step subtracted from the total enthalpy of a number of randomly selected particles. The particle selection is mass weighted, and the gas mass is seen as one single zone. This simplification can cause overlooking of certain phenomena, see ch. 4 on wall quenching.

1.2.3 Flame propagation

In the current SRM code, the amount of mass transferred from the unburned zone to the burnt zone in each time step is determined by a Wiebe function with empirically determined parameters. The Wiebe function describes the burned mass ratio x_b as a function of the crank angle θ according to:

$$x_b = 1 - e^{-a\left(\frac{\theta - \theta_0}{\Delta\theta}\right)^{m+1}}$$

Here, θ_0 denotes the crank angle at which ignition takes place and $\Delta\theta$ is the duration of combustion. In applications, θ_0 typically is set as later than the real ignition timing, since the Wiebe function does not model early flame kernel development well. The parameters a and m describe the overall shape of the Wiebe function. These parameters, as well as the $\Delta\theta$, needs to be adjusted to fit experimental data whenever a model parameter which would affect the flame propagation is changed. The Wiebe function then provides a mass

fraction which for the current time step should be moved from the unburned to the burned zone. It should be noted that despite new particles being created in the burnt zone, no particles are removed from the unburned zone. Instead, the decrease in mass is taken from all particles. The properties of the new particles created in the burned zone reflect the average properties of the unburned zone.

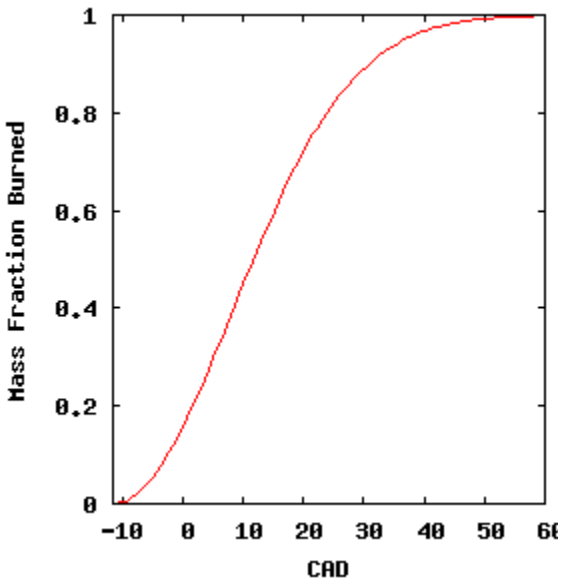

Fig. 2a – Burned mass fraction versus CAD, example of Wiebe function

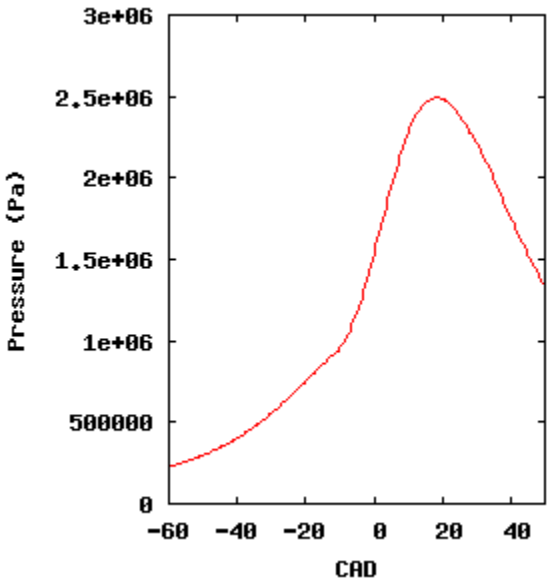

Fig. 2b – Corresponding pressure trace

A typical example of a Wiebe-generated burned mass fraction (MFB) curve is given in fig. 2a. Some clear geometric effects can be seen. During the early phase of combustion, the flame is thought to be growing as a hemisphere, limited by the shape of the cylinder roof. The flame growth is limited first by the piston and later also by the cylinder walls (the relative timing of which of course depends on the spark plug position).

By describing the flame propagation as a function of the laminar flame speed, the turbulence and the cylinder geometry, it should be possible to create a model which (once calibrated) yields predictive results even when individual parameters are changed.

1.3 Underlying assumptions for the flame propagation model

Perhaps the most fundamental assumption of this project is that the flame can be described as spherically expanding. This is certainly not true for all kinds of engines (strong swirl and tumble might distort the flame shape, and advanced engines might make use of stratified combustion to prevent flame-wall contacts) but the assumption is still thought to be reasonable for a large number of applications.

The wall quenching phenomenon – and proposed ways of modelling it – is discussed in ch. 4. The heat loss from the system to the cylinder walls is already included in the SRM model via the Woschni heat transfer method, but its influence on the flame shape is not modelled. In order to limit the extent of this project, the wall quenching was assumed to be generally insignificant except in the very first stage of combustion, where it was simply modelled as a decrease in the speed of flame growth.

Due to the fact that the SRM model is used to study the influence of inhomogeneities in the fuel on engine knock, and that this is done using the same input parameter (the turbulent mixing time, τ) as the turbulent flame propagation (TFP) model, it is important that the required turbulence input in the TFP model is realistic. However, despite that the most realistic representation of τ would be a non-constant value (turbulence at large length scales is created by the piston movement, and dissipates into smaller length scales as two parallel processes), a constant value of τ was used in the validations against experimental data. This was done partly because the flame propagation phase is short enough (20 CAD at 2000 RPM equals 1.7 ms), and partly to avoid the model degenerating into pure curve-fitting. More or less any geometric model could be fitted to experimental data if the turbulence parameters (and hence the flame speed) could be completely freely adjusted. If a decent qualitative agreement with experimental data can be found with the constraint of using a constant τ, the TFP model should produce even more accurate results with a slightly varying turbulent mixing time.

It should be stressed that the underlying library for calculations of the laminar flame speed is only validated for 100% iso-octane. In this thesis, simulations was made for cases using up to 25% n-heptane. It was assumed that if the laminar flame speed deviates significantly, it would be possible to compensate for this deviation by choosing an appropriate turbulence intensity.

2. Turbulence

The concept of turbulence in internal combustion engines is a complicated subject. It's a phenomenon which includes both random and systematic motion on a wide spectrum of both intensity and scale. The gas in motion interacts with the flame front, and in this interaction one needs to take into account such things as the flame thickness and the length scales of the turbulence. The varying relationship between the different parameters means that there is a multitude of ways to describe and model turbulence.

While the kinetic energy contained in a turbulent system usually is located in eddies over a spectrum of sizes, the integral length scale l_L can be used to define the size of the largest of these. In an internal combustion engine, turbulence on this scale is generated by the injection of fuel into the cylinder. The scale and intensity of this turbulence affects both the mixing of fuel and oxidizer and the flame propagation. The flame propagation speed is dependent on the ratio between the integral length scale and the flame thickness δ_L (which can be defined either by the momentary distribution of species, or by thermodynamic properties). The smallest scale of turbulence is described using the Kolmogorov scale, l_K [3].

The turbulence intensity, u', is measured as the root-mean-square value of the particle speed deviation from the flow speed of the gas. The turbulent flame propagation depends on the ratio between the turbulence speed and the laminar flame propagation speed S_L. The quantity u' is assigned in the SRM code via the turbulent mixing time $\tau = l_L/u'$ In a

three-dimensional system, assuming homogeneous and isotropic turbulence, it is possible to calculate the turbulence speed from the turbulent kinetic energy according to $k=3u'^2/2$.

Using the concepts mentioned above, one can define a turbulent Damkohler number as

$$Da=\frac{S_L l_L}{u'\delta_L}$$

and using a Kolmogorov velocity scale u_K, a Karlovitz number as

$$Ka=\frac{\delta_L^2}{l_K^2}=\frac{u_K^2}{S_L^2} \quad .$$

The Karlovitz number connects the flame thickness to the small scale Kolmogorov turbulence. It might also be useful to define a turbulent Reynolds number as

$$\mathrm{Re}=\frac{u' l_L}{S_L \delta_L} \quad .$$

With above definitions, and using l_δ to denote the thickness of the fuel consumption layer of the flame (also called the inner layer), one can map the different regimes for premixed turbulent combustion. In Fig. 3, this map and the expected area where internal combustion engines typically operate is displayed.

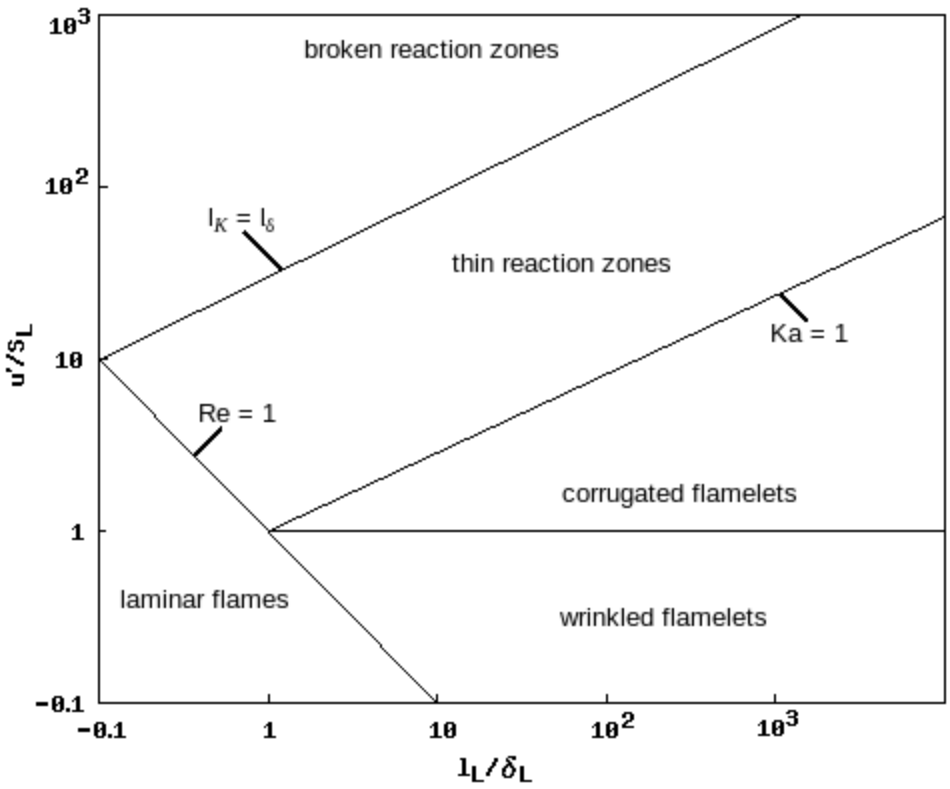

Fig. 3 – Combustion regions for premixed turbulent combustion

Intuitively, u' and l_L should evolve during the engine cycle. The kinetic energy in the eddies of the integral length scale is thought to dissipate into smaller eddies. The SRM model allows for an input of a time-dependent turbulent mixing time $\tau = l_L/u'$, but for simplicity it is assumed constant throughout the validation. The time-dependency of τ is important for precise modelling of the mixing, and can be determined by CFD calculations. Since this thesis mainly concerns the flame propagation, which typically takes in the region of a few ms, the turbulent mixing time is kept invariant.

2.1 Simple turbulence models

Numerous attempts have been made to find an adequate model for describing turbulent flame propagation [4,5], with varying degrees of ambition. One of the most fundamental

parameters for describing turbulence is the RMS value of the gas particles' deviation from the average speed, *u'*. Many simple models are only dependent on *u'* as an input parameter, and in some cases one or two more parameters. These models can provide good results for a particular system once they are empirically “tweaked” to data from that system. However, when applied to other systems than the ones they were calibrated to, they tend to produce rather bad predictions.

These simple turbulence models are still very useful, since very rarely a complete set of data is available regarding the turbulence in the system. Assuming that all unknown parameters are invariable, and then performing curve fitting to an expression of only the known parameters can be an effective way to understand the behaviour of a specific system.

Typical examples of this group of turbulence models are found in Norbert Peters *Turbulent Combustion* [4] (Eq. 4) and in an article by Nilsson & Bai [5] in 2002 (Eq. 5).

$$\frac{S_T}{S_L} = 1 + C\left(\frac{u'}{S_L}\right)^n, 0.5 < n < 1 \quad [4]$$

$$\frac{S_T}{S_L} = 1 + 0.46\left(\frac{u'}{S_L}\right) + 0.2\left(\frac{u'}{S_L}\right)^{1/2} \quad [5]$$

2.2 Analytical turbulence model

The *Kolmogorov-Petrovski-Piskunov* (KPP) theorem states that if the balance equation $u_t = u_{xx} + f(u)$ for a propagating flame has a continuous spectrum of solutions at the flame leading edge, the turbulent flame propagation speed is the minimum of those solutions. In 2008, Kolla, Rogerson, Swaminathan and Chakraborty [6] used KPP analysis to derive an expression for S_t, using the derived expression to validate their model for the scalar dissipation rate ε_c.

With a reaction rate of ω, the balance equation for a steadily propagating turbulent flame is:

$$\rho_u S_T \frac{\partial \tilde{\Theta}}{\partial x} = \bar{\rho} \frac{\nu_t}{Sc_c} \frac{\partial^2 \tilde{\Theta}}{\partial x^2} + \bar{\dot{\omega}} \quad [6]$$

where the average reaction rate is

$$\bar{\dot{\omega}} = \frac{2}{(2C_m - 1)} \rho \epsilon_C \quad [7].$$

Above, Θ is the reduced temperature (having a value of 0 for unburned fuel and 1 for burned, thereby behaving similarly to a progress variable), S_T is the turbulent flame propagation speed, Sc_C is the Schmidt number for the progress variable c ($Sc_C \approx 1$), ν_t is the turbulent viscosity and C_m is related to c through the definition

$$C_m \equiv \frac{\int c \dot{\omega} p(c) dc}{\int \dot{\omega} p(c) dc} \quad [8].$$

p(c) above is the probability density function of c, and C_m has a typical value of 0.7.

The expression for the scalar dissipation rate which Kolla et al. intended to test was

$$\epsilon_c \simeq \frac{1}{\beta'} (2K_c^* \frac{S_L}{\delta_L} + [C_3 - \tau C_4 Da_L] \frac{\bar{\epsilon}}{\bar{k}}) \overline{c''^2} \quad [9].$$

Note that $\bar{\epsilon}$ above is the average dissipation rate of turbulent kinetic energy, which can be written as $\bar{\epsilon} = \frac{u'^3}{l_L}$ [10].

Da_L is the local Damkohler number, given by

$$Da_L = \frac{S_L / \delta_L}{\bar{\epsilon} / \bar{k}} \quad [11]$$

and τ is the heat release parameter, defined as $\tau = (T_{ad} - T_u)/T_u$ (not to be confused with the turbulent mixing time τ used in the SRM model).

Combining equations [7] and [8] gives us

$$\bar{\dot{\omega}} = \frac{2}{2C_m - 1} \rho \frac{1}{\beta'} (2K_c^* \frac{S_L}{\delta_L} + [C_3 - \tau C_4 Da_L] \frac{\bar{\epsilon}}{\bar{k}}) \overline{c''^2} \quad [12].$$

The KPP analysis consists of finding the minimum solution of the balance eq. [6]. The discriminant of the equation is

$$\Delta = S_T^2 - 4\frac{\nu_t}{Sc_c}\cdot\left(\frac{\partial \omega}{\partial c}\right)_{c\to 0} \quad [13]$$

and hence the balance equation has solutions for

$$S_T \geqslant 2\sqrt{\frac{\nu_t}{Sc_c}\cdot\left(\frac{\partial \omega}{\partial c}\right)_{c\to 0}} \quad [14].$$

For the flame leading edge $c''^2 \approx c(1\text{-}c)$, and the KPP theorem gives

$$S_T = \sqrt{4\frac{\nu_t}{Sc_c}\cdot\frac{2}{(2C_m-1)}\frac{1}{\beta'}\left(2K_c^*\frac{S_L}{\delta_L}+[C_3-\tau C_4 Da_L]\frac{\bar{\epsilon}}{\bar{k}}\right)} \quad [15].$$

Using equations [10] and [11] with k defined as

$$\bar{k} = \frac{3u'^2}{2} \quad [16]$$

and the turbulent viscosity ν_t defined as

$$\nu_t = \frac{C_\mu \bar{k}^2}{\bar{\epsilon}} \quad [17]$$

we get:

$$S_T = \sqrt{\frac{18\,C_\mu}{(2C_m-1)\beta'}u' l_L\left(2K_c^*\frac{S_L}{\delta_L}+C_3\frac{2}{3}\frac{u'}{l_L}-\tau C_4 Da_L\frac{2}{3}\frac{u'}{l_L}\right)} \quad [18]$$

$$S_T = \sqrt{\frac{18\,C_\mu}{(2C_m-1)\beta'}u' l_L\left(2K_c^*\frac{S_L}{\delta_L}+C_3\frac{2}{3}\frac{u'}{l_L}-\tau C_4\frac{S_L}{\delta_L}\right)} \quad [19]$$

$$S_T = \sqrt{\left(\frac{18\,C_\mu}{(2C_m-1)\beta'}\right)\left([2K_c^*-\tau C_4]\frac{S_L u' l_L}{\delta_L}+C_3\frac{2}{3}u'^2\right)} \quad [20]$$

$$\frac{S_T}{S_L} = \sqrt{\left(\frac{18\,C_\mu}{(2C_m-1)\beta'}\right)\left([2K_c^*-\tau C_4]\frac{l_L}{\delta_L}\frac{u'}{S_L}+C_3\frac{2}{3}\left(\frac{u'}{S_L}\right)^2\right)} \quad [21].$$

In [6], eq. 21 was used to predict the behaviour of turbulent flames in a wide spectrum of experimental data, generally with good results compared to other turbulence models.

2.3 Simplified analytical approach

The formula of Kolla et al. has shown promising [7], but it is far too complex for the task at hand. By simplifying it, one could arrive at an expression allowing users to easily tweak the model to fit their system (as the more simple models), but still makeing it possible to adjust a large array of turbulence parameters to see how they individually affect the combustion.

When Eq. 21 is expanded using adequate definitions of C_3 and C_4 [6], we get:

$$\frac{S_T}{S_L}=\left(\frac{18C_\mu}{(2C_m-1)\beta'}\left[2K_C^*-\tau\cdot 1.1\left(1+\left(\frac{u'}{S_L}\right)^{1.5}\left(\frac{\delta_L}{l_L}\right)^{0.5}\right)^{-0.4}\right]\left(\frac{u' l_L}{S_L\delta_L}\right)+\frac{18C_\mu}{(2C_m-1)\beta'}\cdot\frac{2}{3}\cdot\frac{1.5\cdot\left(\left(\frac{u'}{S_L}\right)^{1.5}\left(\frac{\delta_L}{l_L}\right)^{0.5}\right)^{0.5}}{1+\left(\left(\frac{u'}{S_L}\right)^{1.5}\left(\frac{\delta_L}{l_L}\right)^{0.5}\right)^{0.5}}\cdot\left(\frac{u'}{S_L}\right)^2\right)^{1/2}$$

[22]

The values of $C\mu$, C_m and β' are given in the articles of Kolla et al. as $C_m \approx 0.7$, $C\mu = 0.09$ and $\beta' = 6.7$. K_C* is dependent of the flamelet structure, and is found to be roughly 0.85τ for methane [6], with a slight dependency (in the region of ±10%) on the equivalence ratio. K_C* for iso-octane has not been determined, but the relationship between K_C* and τ is thought to be of a similar order of magnitude for most fuels. By using the following definitions:

$$d=\frac{18C_\mu}{(2C_m-1)\beta'}\approx 0.6045 \quad [23]$$

$$a=1.1\cdot d \quad [24]$$

$$b\approx 1.6\cdot d \quad [25]$$

(where the exact relationship between b and d depends on the relationship between K_C* and τ) we can simplify Eq. 22 to

$$\frac{S_T}{S_L}=((b-a\cdot(1+(\frac{u'}{S_L})^{1.5}(\frac{\delta_L}{l_L})^{0.5})^{-0.4})\frac{T_{ad}-T_u}{T_u}\cdot\frac{l_L}{\delta_L}\cdot\frac{u'}{S_L}+\frac{d}{(\frac{u'}{S_L})^{0.75}+(\frac{\delta_L}{l_L})^{-0.25}}\cdot(\frac{u'}{S_L})^{2.75})^{1/2} \quad [26].$$

All parameters except *a*, *b* and *d* (and the turbulence input parameters u', δ_L and l_L) are already calculated in the SRM code. *a*, *b* and *d* have approximate values according to Eqs. 23-25, but they can be modified to give optimal predictions for the engine in question.

In both the fully analytical model and the simplification, $S_T/S_L \rightarrow 0$ when $u'/S_L \rightarrow 0$. Trivially, the turbulent flame speed should get closer to the laminar flame speed the more the turbulence intensity decreases, something which is seen in other models such as Eqs. 4 and 5. The reason the analytical model of Kolla et al. does not follow this behaviour is that they in the KPP analysis assume that the significant part of turbulent kinetic energy comes from large scale turbulence (in the size of the integral length scale), whereas for low turbulence a large portion of the energy might be found on the small Kolmogorov scale. In this application, we need to cut the formula off below a suitable position, merging it with a simple model. Preferably, the program should fit one of the simpler models to the analytical one (with given parameters), resulting in a smooth transition in the cut-off point.

3. Cylinder geometry

The shape of the cylinder and the placement of the spark plug, have significant effects on the combustion process. Typically, a car engine is designed with a concave cylinder top and the spark plug placed somewhat off centre of the cylinder's longitudal axis.

The cylinder top could for simplicity be approximated as a cone, but the exact size and shape of that cone would need to be individually tweaked for each engine. Instead, I have opted for using a Monte Carlo model for calculating the flame volume as a function of

the flame radius, requiring the user to provide input describing the cylinder profile. This approach should make it possible to simulate the effect of changes in the cylinder geometry such as a variation in spark plug location. Unfortunately, the experimental data available for validation was for fixed geometries, and thus it is only possible to assess that changes in the modelled geometry reflect the same trends as one would expect from theory.

3.1 Monte Carlo model

During the course of the project, it became apparent what level of precision was needed in the geometry modelling and the Monte Carlo algorithm was developed accordingly. At the beginning of the project, it was believed that sufficient accuracy could be reached by performing analytical calculations of flame volume based on either a flat or a cone shaped cylinder head. The Monte Carlo calculations were introduced early in the project, but for speed and simplicity it was originally only used to simulate rotationally symmetric geometries and flat piston surfaces.

At that stage, the geometry input consisted of a set of two dimensional coordinates, defining an intersection of the cylinder head and the spark plug position (See Fig. 4). For complex geometries with the spark plug located close to the cylinder centre, a profile could be defined as an approximation of the cylinder head. It was important still to have the same clearance height and volume as the simulated engine, in order to catch the effects of flame-piston contact.

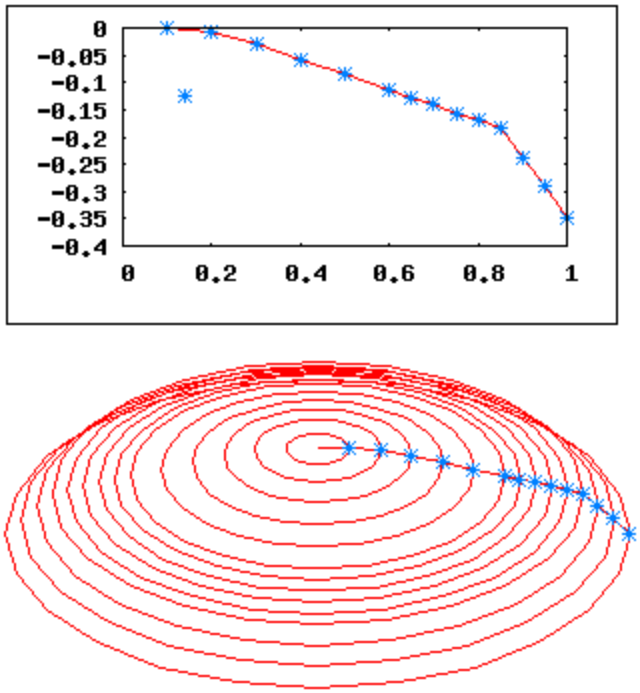

Fig. 4 – Visualisation of the geometry input for simulation of a rotationally symmetric cylinder head

During validation (see particularly Ch. 6.3.2), it became clear that neither the approximation of rotational symmetry nor that of a flat piston surface produced results with the desired accuracy. The model was modified to allow for a fully three-dimensional input of the cylinder head and a non-flat but rotationally symmetric piston surface. The symmetry requirement for the piston was chosen to keep the algorithm as fast as possible and because the piston in question (the particular case was the 2 l engine described in Ch. 6.3.2) fulfilled the requirement. In the future, it is possible to develop an algorithm similar to that of the cylinder roof in order also to be able to model asymmetric pistons.

The Monte Carlo volume is defined as a cube with sides twice the size of the flame radius and centred at the spark plug for flame radii smaller than or equal to the cylinder radius and as a cuboid with sides twice the cylinder radius and height according to the flame radius plus the vertical spark plug offset for flame radii larger than the cylinder radius. For a given flame radius, a number of random three dimensional points is assigned within

the Monte Carlo volume and the fraction of points which are within the cylinder boundary conditions and within the flame radius from the spark plug, gives a shape factor used to calculate the flame volume.

When the flame propagation step is reached in the time step loop, a new flame radius is calculated based on the current flame volume and piston position. The flame radius is increased according to the turbulent flame propagation speed and the size of the time step, and a new flame volume is calculated.

4. Wall quenching

The implementation of the Woschni heat transfer correlation described in chapter 1.2.3 means that the heat exchange with the cylinder walls over multiple time steps is distributed statistically evenly over the cylinder gas (though with stochastic variations in each time step based on the random selection of particles to exchange heat with the walls). This however overlooks some systematic behaviour, for example the wall quenching phenomenon. When a large (>80%) portion of the cylinder mass is burned, all unburned fuel left will be located near the cylinder walls. The increased cooling of this gas means that there tends to be a fraction of the fuel mixture which is never burnt, typically in the region of one to five percent. The wall quenching can also distort the presumed spherical shape of the flame.

Letting the model burn all mass causes the decline of the pressure curve to occur with a slight delay compared to experimental data. The simplest way to avoid this would be to let the user specify a limit after which the mass transfer from the unburned to the burned zone is stopped. However, this is not a very appealing approach.

One approach that was tried was to describe the transferred mass in each time step not just using the increase in volume for a certain increase in flame radius, but as a function

of that volume and the added volume which was within a certain distance from the cylinder walls. This model would serve to limit the burning speed in the last phase of combustion, but would still fail to model the incomplete combustion of the fuel mixture. The fraction of the added volume within a certain distance from the cylinder walls will generally be substantially smaller than the defined Monte Carlo space, with the consequence that an increased number of Monte Carlo points would be needed to control the influence of stochastic variations. The increase in CPU time is not justified by the minor implication this approach has for the model behaviour.

A more realistic model could be achieved by using the Monte Carlo algorithm to calculate the fraction between the total zone volume and the volume of the zone within a certain distance from the cylinder walls, for each zone consecutively. Then in the Curl mixing routine, a number of particles – based on this volume fraction and the total number of particles in the zone – could be introduced with a temperature equal to that of the cylinder walls. Either one could introduce “pseudo-particles” working as a heat reservoir or one could change the temperature of a number of existing particles. When all or most of the unburned zone is located close to the cylinder walls, this would result in a slowed down flame propagation. The effect would be to both replace the Woschni heat transfer and to produce the most realistic possible modelling of wall quenching. The time span of this thesis does not allow for the development, tweaking and validation of this kind of model, but the Monte Carlo code has been prepared for it. For optimal precision, one could also model the crevice volumes of the combustion chamber, where fuel mixture is left unburned even in the case of autoignition.

Besides the incomplete combustion, wall quenching is relevant for the early flame development. This coincides with the stochastic early flame kernel development and the gradual introduction of a turbulence effect with flame surface area, and the resulting behaviour is very complex to model. By linearly increasing the flame propagation speed from the laminar to the turbulent flame speed – up to a flame radius set as a user parameter – good experimental correlation was found in all validation cases. The suitable

limit for the flame radius was found to be roughly half the integral length scale.

6. Validation

6.1 Sensitivity

Though Eq. 26 contains a number of parameters which will supposedly be unknown to the end user of the model, many of them are approximately constant for a large range of operating points. Once familiar with the model, any user of the SRM code should relatively quickly be able to find fitting parameters for a particular engine. A sensitivity study was performed, varying the individual parameters within the same order of magnitude as the difference between the various validation cases (see Ch. 6). Table 1 below contains default, max and min values which were used for the different parameters.

The laminar flame thickness δ_L is dependent on the pressure and the fuel. Variations due to pressure changes within the cycle are thought to be small enough for δ_L to be approximately constant. A value of 0.6 mm gave well-fitting results to all validation cases. Fig. 5 and 6 show typical cases (hemispherical cylinder roof, off-centre spark plug, 1200 RPM) for three different values of the laminar flame thickness; 0.4 mm, 0.6 mm and 0.8 mm. The pressure traces are displayed in fig. 5 and the variations in the behaviour of Eq. 26 are shown in Fig. 6. The relevant region for u'/S_L is between 0.5 and 1. This is of interest because the global trend is for S_L to increase during the entire combustion phase, so u'/S_L decreases. The inclination and to some extent the linearity of the curve in fig. 6 in the relevant region thus decides the relationship between flame propagation speeds in the early and late stage of combustion. This can be used to ensure that tweaking the model has resulted in finding the correct parameters, not just any of the many combinations which give the correct flame propagation speed at a given point in time. It should be noted that the term $(T_{ad} - T_u) / T_u$ in eq. 26 is not strictly constant over time, but is taken as an average value in the early stage of combustion for the creation of the S_T/S_L

data plots.

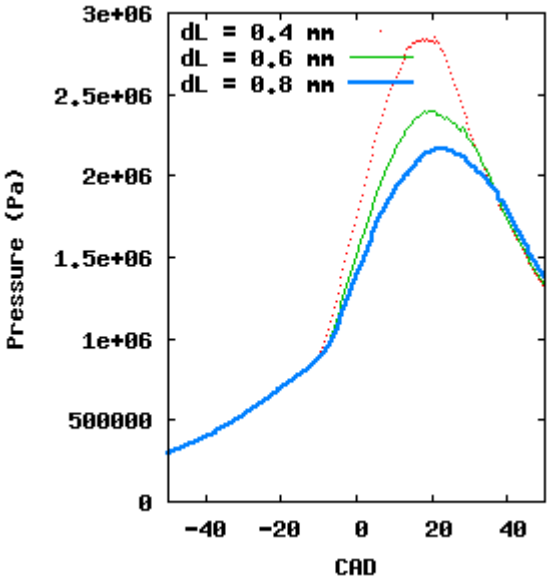

Fig. 5 – Pressure comparison for δ_L = 0.4, 0.6 and 0.8 mm

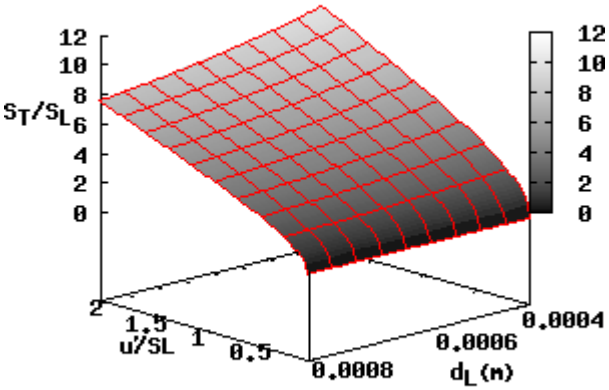

Fig. 6 – S_T/S_L versus u'/S_L for a sweep of δ_L values

The behaviour of eq. 26 depends on the ratio between l_L and δ_L rather than their individual values, so varying l_L is presumed to have an effect similar to that of varying δ_L. The suitable integral length scale is often taken as half the engine bore where more precise CFD calculations are unavailable, though in the current S_T model, the most realistic results seem to be reached with a slightly lower value. For this hypothetical case, a bore of 96 mm was used, with length scales of 35, 40 and 45 mm. As with the laminar flame thickness, Fig. 7 and 8 show the acquired pressure traces and the dependency between S_T/S_L and u'/S_L.

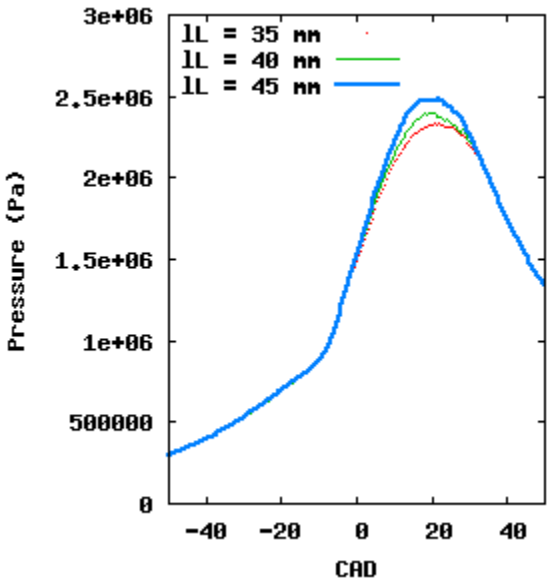

Fig. 7 – Pressure comparison for integral length scales of 35, 40 and 45 mm

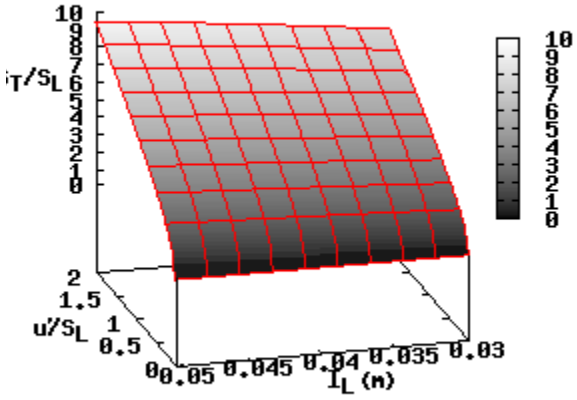

Fig. 8 – S_T/S_L versus u'/S_L for a sweep of integral length scales

The turbulence velocity *u'* is the parameter which will typically have the largest variations, especially for different engine speeds since the piston movement is an important factor in the creation of turbulence in the gas. The two validation cases in chapter 6.3.1 and 6.3.2 were running at 1200 RPM and 2500 RPM. Suitable values for *u'* was found to be 0.625 m/s and 3.42 m/s respectively. For maximum brake torque in the default case of this sensitivity study, u' was set to 1.00 m/s. Turbulence velocities at 0.75, 1.00 and 1.25 m/s were investigated. See Fig. 9 and 10 for pressure traces and mass fraction burned curves.

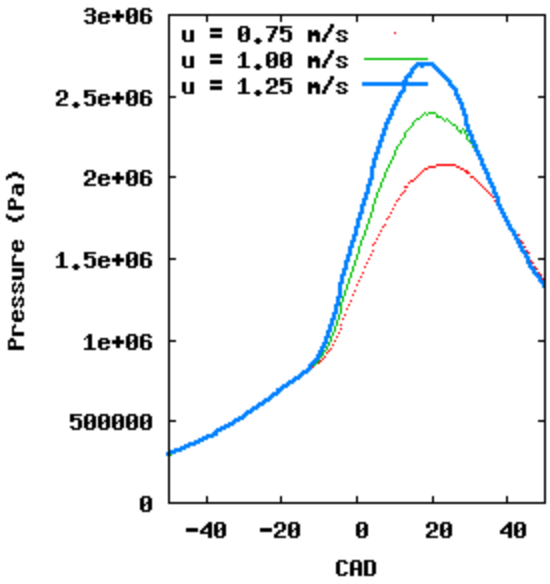

Fig. 9 – Pressure comparison for variations in the turbulence speed u'

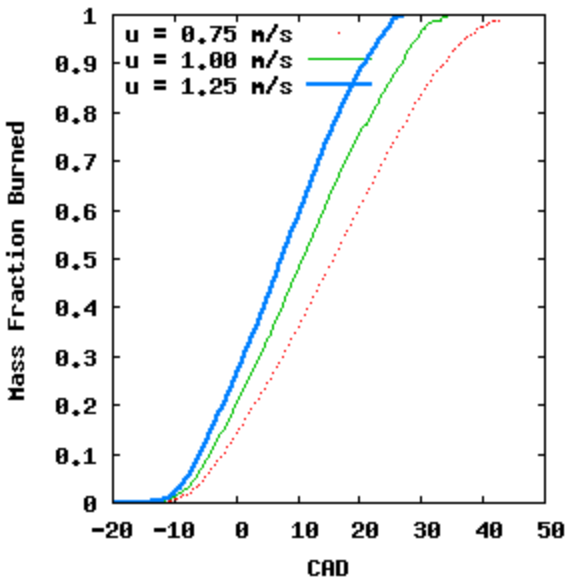

Fig. 10 – Burned mass fraction for varied u'

While Chapter 6.2 demonstrates the variations in behaviour for different cylinder geometries, studies were also made to showcase the model sensitivity to spark plug position. In this study, a spark plug offset of 24 mm from the centre of the cylinder has been used. Fig. 11 shows the pressure traces for offsets of 12, 24 and 36 mm, while Fig. 12 shows the burned mass fraction as a function of time (measured in CAD). Fig. 13 displays the relationship between enflamed volume and flame radius. A notable effect in Fig. 12 and 13 is the decrease in burning ratio when the flame has made contact with the cylinder walls, and also when flame-piston contact is reached between -10 CAD and TDC. Due to the hemispherical shape of the roof, flame-piston contact happens at a lower flame radius for more off-centre spark plugs. This effect would also vary with the ignition timing, which was kept constant in these cases.

It should also be noted that with a small offset the combustion is considerably faster. Typically with a setup similar to the one used in this sensitivity study and a spark plug close to the cylinder centre, one would also have a later point of ignition than that which has been used in this case.

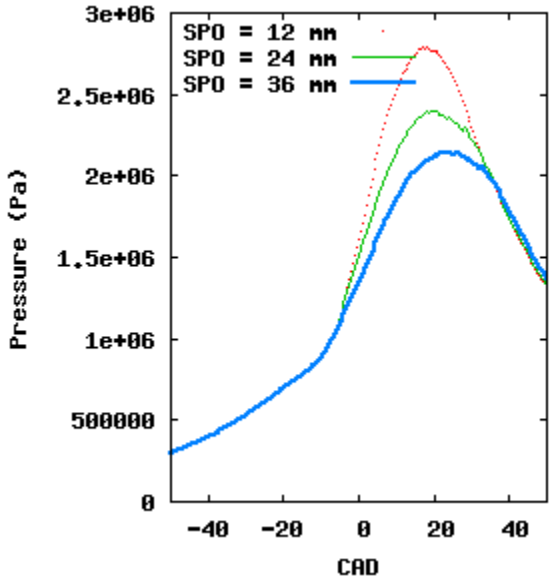

Fig. 11 – Pressure comparison for spark plug offsets of 12, 24 and 36 mm from the cylinder centre

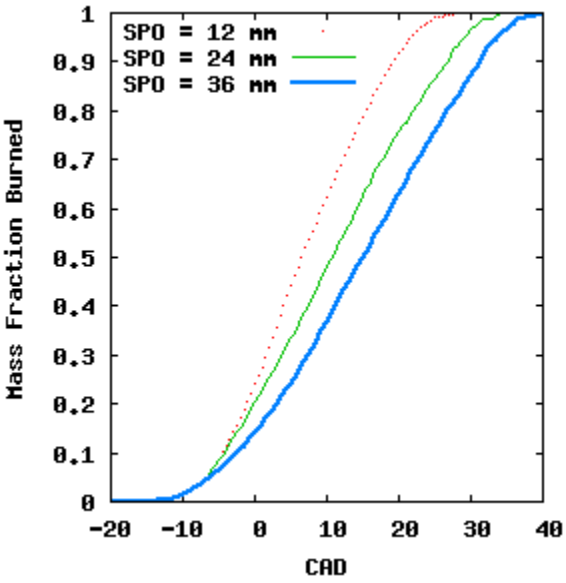

Fig. 12 – Burned mass fraction for varied spark plug placement

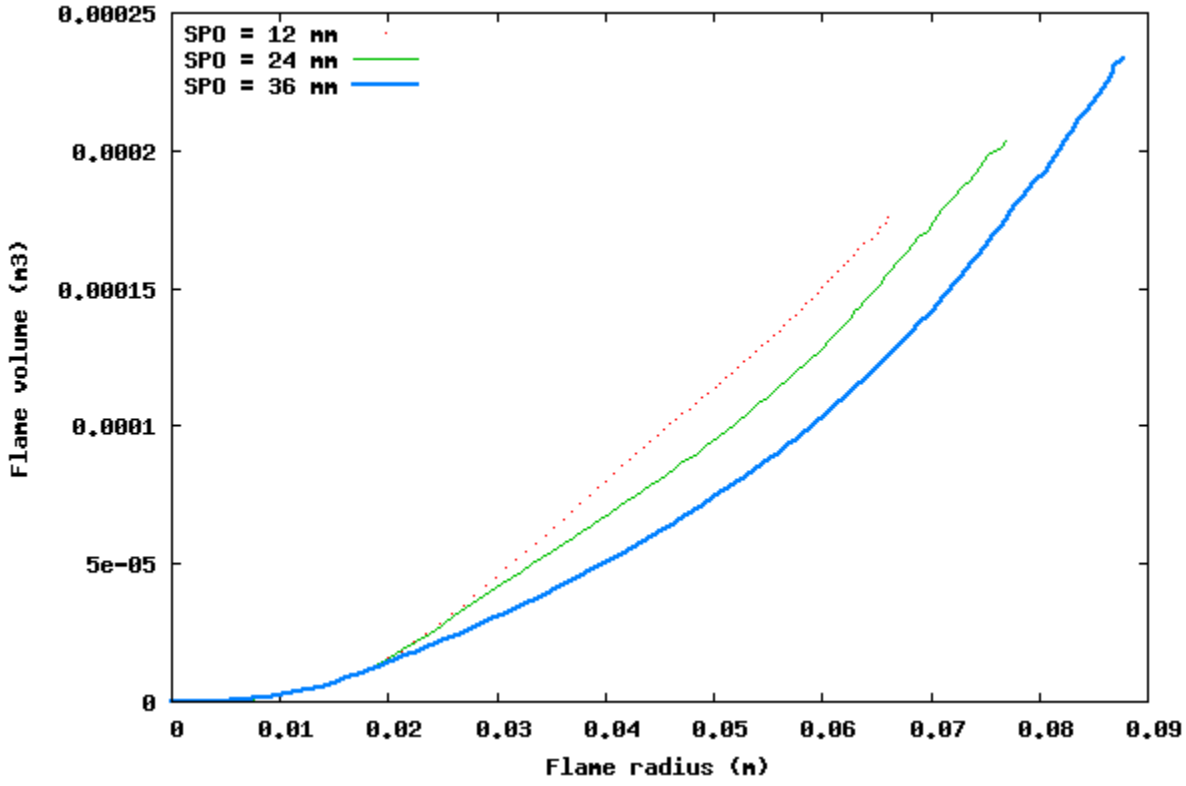

Fig. 13 – The relationship between flame radius and enflamed volume, depending on spark plug location

In Eq. 26 the only non-phenomenological parameter which needs adjusting is *b*, which should vary with the equivalence ratio (the ratio between fuel and air, defined as 1 at stochiometric conditions) and fuel. For all tested cases with Φ = 1.0, good agreement was found using *b* = 0.805. To demonstrate the sensitivity of this parameter, test cases were simulated using *b* = 0.790 and *b* = 0.820. For equivalence ratio deviations of about ±10-20%, that is the corresponding region in which *b* is expected to be located. Note that this sensitivity study used Φ = 1.0 in all cases including these. In order to simulate cases with different equivalence ratio, both Φ and *b* should be adjusted accordingly.

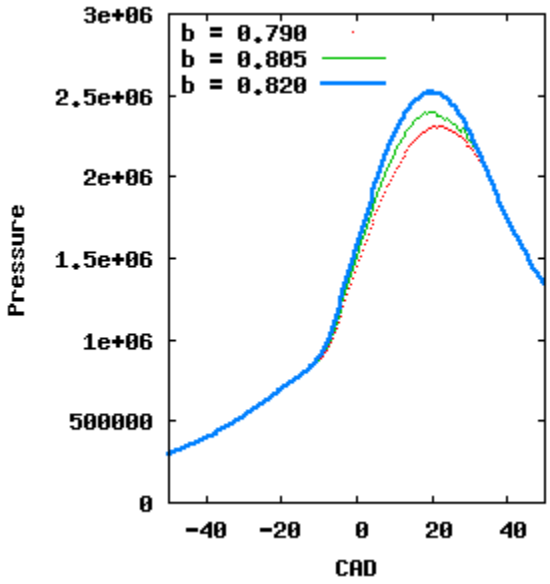

Fig. 14 – Pressure comparison for variations in equation parameter b

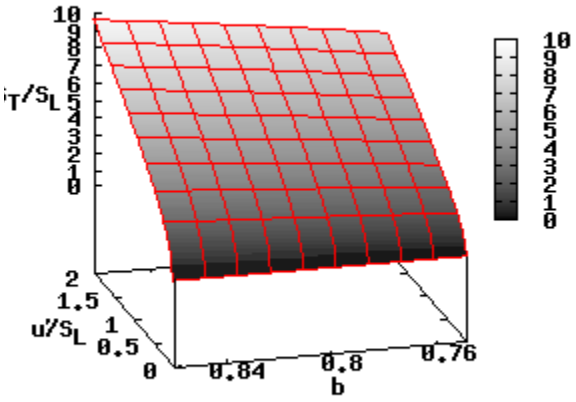

Fig. 15 – S_T/S_L as a function of u'/S_L for a sweep of values of b

To emulate the settings of a typical engine, the ignition timing was set so that the case with default parameters (see table 1) reached 50% burned mass around 10 CAD, meaning a start of combustion at 20 CAD BTDC. The modelling of the flame kernel development is rather crude, and this (plus stochastic inhomogeneities in the gas) might be simulated though variation of the model's ignition timing. Fig. 16 and 17 show the pressure trace and burned mass fraction for ignition timings at -17, -20 and -23 CAD.

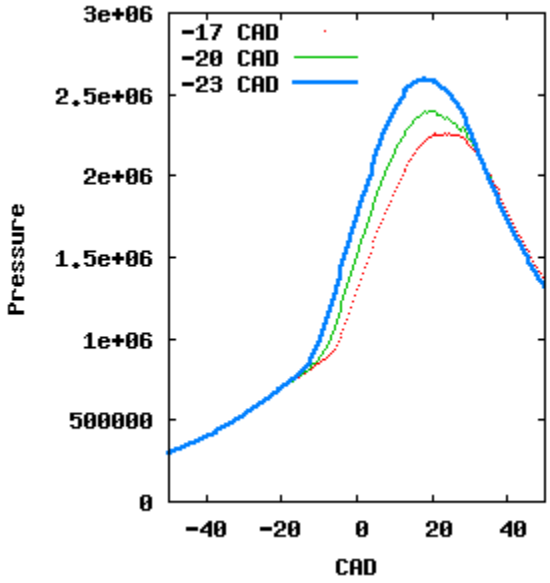

Fig. 16 – Pressure trace for ignition timing of 17, 20 and 23 CAD BTDC

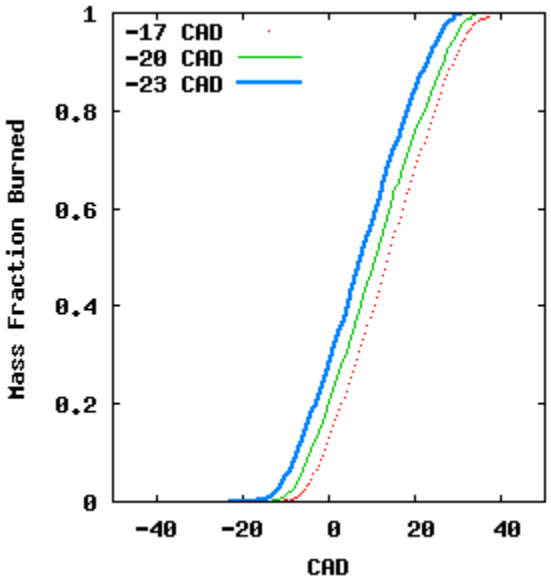

Fig. 17 – MFB curves for varied ignition timing

Finally, Table 1 contains the default, max and min values used in the sensitivity study.

Parameter	Min	Default	Max
δ_L	0.4 mm	0.6 mm	0.8 mm
l_L	35 mm	40 mm	45 mm
u'	0.625 m/s	1.0 m/s	3.42 m/s
b	0.790	0.805	0.820
Spark plug offset	12 mm	24 mm	36 mm
Ignition timing	17 CAD BTDC	20 CAD BTDC	23 CAD BTDC

Table 1

6.2 Geometry

In order to do a complete validation of the geometry model, one would need specialised experimental data for identical engines with varying cylinder heads/spark plug placement. In the absence of this kind of data, comparative verification was performed against a study by Poulos and Heywood [8]. This study made use of a quasi-dimensional combustion model coupled with a Monte Carlo geometry to – amongst many other things – study the effect of cylinder geometry on flame propagation. Due to significantly higher computational times in 1983, the study of Poulos and Heywood set out to identify general geometrical tendencies rather than to produce detailed descriptions of the various phenomena observed, and possibly to showcase the applicability of the concept.

The amount of information on both engine operating conditions and the exact geometries evaluated in [8] is insufficient for allowing for exact replication of the case, but an attempt has been made to reconstruct a case as similar as possible.

Fig. 18 shows the average mass burning rate (in percent of the total mass per crank angle degree), effectively a burn speed normalised to the total gas mass. The burning rates have been calculated for three combustion regions; 0-10% of the initial fuel burned, 10-90% burned and 0-90% burned. Good general agreement is found with [8], with the major discrepancy for the flat cylinder top with a central spark plug. The fact that the models show similar results in the early combustion region indicates that the difference in the 10-90% region is caused by flame-piston contact. The exact nature of the piston contact is determined by the ignition timing and the distance between the spark and the cylinder roof, both of which were unaccounted for in [8].

The regions studied in this chapter and in [8] were chosen because of difficulties in modelling the final stage of combustion. However, the model used in [8] does not seem to account for flame kernel development, possibly even more challenging to model correctly. For an optimal comparison, the burn angle ratios from the SRM model in Fig.

18 are calculated from 0.01% burned mass rather from the ignition timing used as model input.

For cylinders with hemispherical roofs, a spark plug location far to the side of the cylinder should result in a comparatively slow combustion during the entire process. With the spark plug positioned in the centre of the cylinder, or with the spark plug positioned of a distance about half the cylinder radius from the centre, the initial burn ratio should be similar, but the chamber with a centred spark plug should have a significantly faster burn ratio in the later stages of combustion due to a later flame-piston contact. The geometry model follows this general behaviour, as seen in Fig. 18.

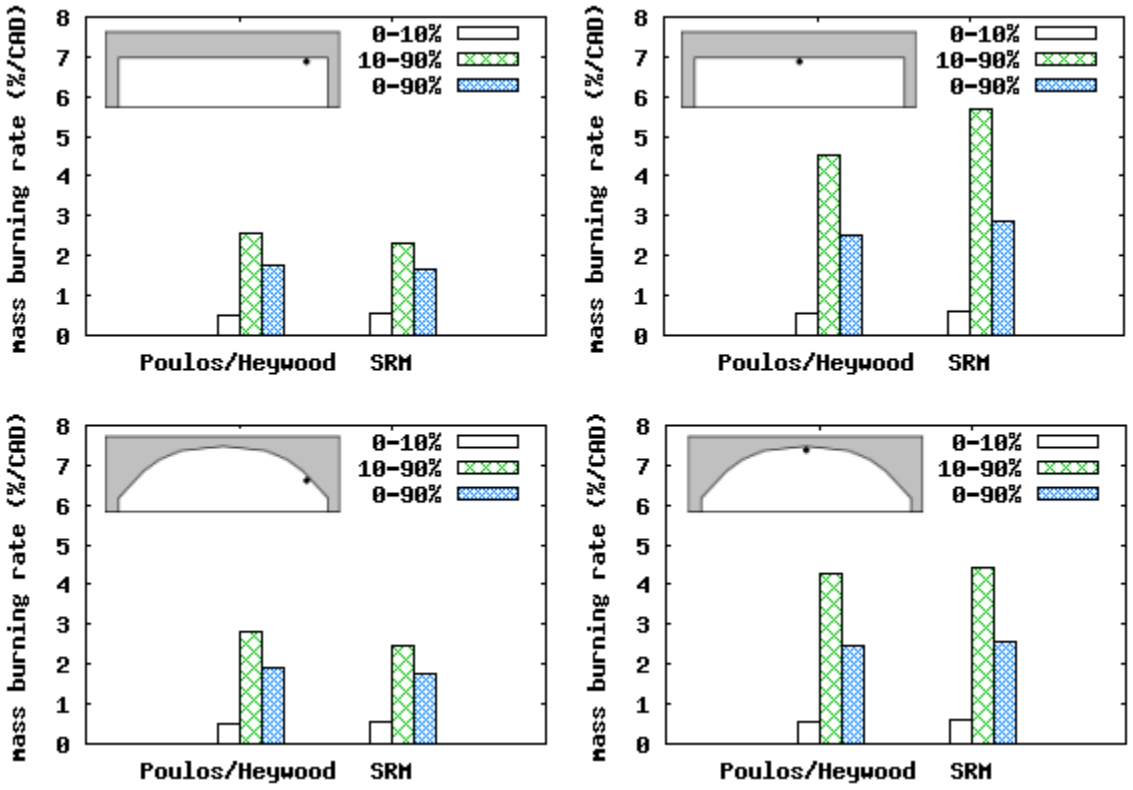

Fig. 18 – Comparison between model predictions and predicted burn angle ratios by Poulos & Heywood [8]

6.3 Flame propagation model

6.3.1 Chalmers horse shoe engine

The developed model's ability to predict autoignition has been validated against pressure data from an experimental engine equipped with a horse-shoe shaped cylinder top and double spark plugs according to Fig. 19, located at Chalmers University of Technology in Gothenburg. Average pressure had been measured over several cycles, and individual pressure traces were available for knocking cases. The temperature data, however, was limited to average post-ignition temperatures. The experimental data covers five different equivalence ratios Φ, ranging from 0.77 to 1.28. Table 2, at the end of this chapter, contains the engine parameters of this case.

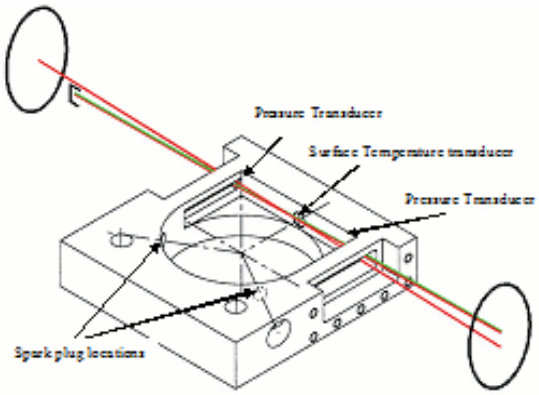

Fig. 19 – Drawing of horse-shoe shaped cylinder top with double spark plugs

Neither the cylinder platform nor the double spark plug setup can be strictly modelled without modification of the Monte Carlo model. However, assuming a spherical flame propagation the two flames propagating from the two spark plugs would have a shape and a volume/radius ratio resembling that of two quarter-spheres in the initial stage of combustion. When the flame radius is larger than half the distance between the spark plugs, the volume/radius ratio would tend towards that of a quarter-sphere. The Monte Carlo model can be made to simulate this behaviour by assuming a regular flat cylinder

top with a single spark plug placed at a 9 mm offset from the cylinder centre. The distance from the cylinder walls would be 39 mm, about equivalent to half the distance between the spark plugs in the Chalmers engine. This approach does not account for the horse shoe-shaped crevice volume, but we expect autoignition to occur before the flame front has reached this volume. Another inaccuracy is that the calculated piston position for a given cylinder volume will be somewhat incorrect when the crevice is neglected, resulting in an incorrectly calculated piston/flame contact. This can be compensated for by slight adjustments of the turbulence speed u' (and hence the flame propagation speed), but it could lead to minor discrepancies between the early (before flame/piston-contact is reached) and middle region of combustion.

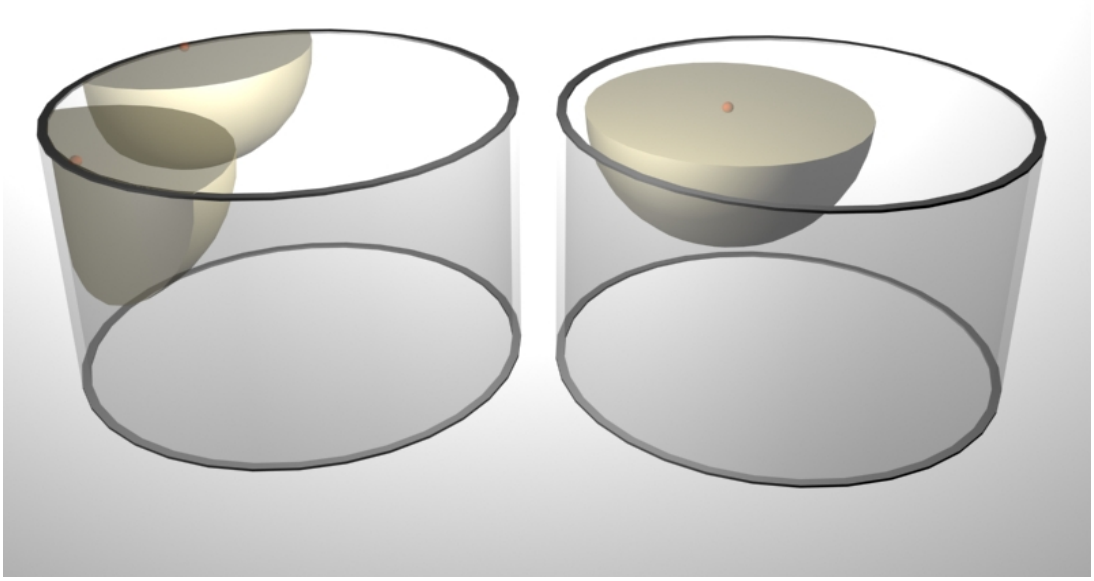

Fig. 20 – Visualisation of the flame shape at flame radii of 30 mm in the experimental engine, compared to that of a simplified one-plug approach with rotational cylinder symmetry

Fig. 21 shows the model output compared to the experimental pressure trace for Φ = 1.00. Autoignition occurs at 15 CAD ATDC, with a flame radius in the region of 45 mm.

The approximation of the flame shape is thought to be mostly correct up to radii of 39 mm, and the radius/volume relationship should then slowly deviate from that of the experimental setup with increased radii. Good correlation can be found, suggesting both that the geometry approximation is valid and that the required u' in the TFP model is consistent with the required τ in the mixing model. In cases where autoignition is reached, the pressure after autoignition is typically higher in the model output than in the experimental data. This is because the SRM code burns all the fuel, whereas in real life some fuel is left unburnt through crevices in the cylinder.

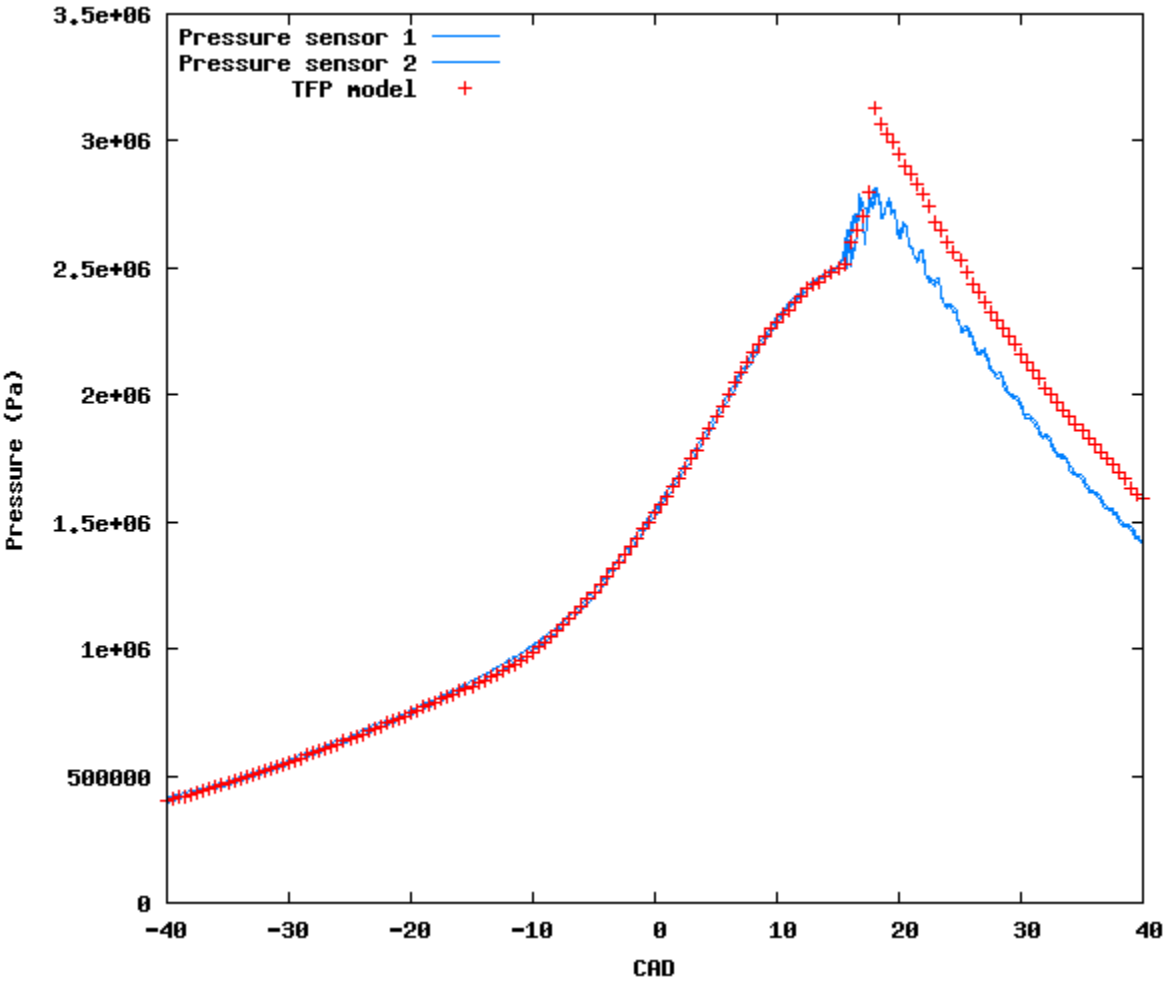

Fig. 21 – Pressure traces for TFP model and experimental data. Φ = 1.00, b = 0.805

The results in fig. 21 were obtained using a value of u' = 0.625 m/s, a laminar flame thickness of 0.6 mm and an integral length scale of 4.0 cm. Note that the value used for the integral length scale is lower than the expected approximate value (usually taken as half the engine bore, in this case 48 mm)

The equation parameters used in the turbulence model for fig. 21 are a = 0.66, b = 0.805 and d = 0.6. This should be compared to a = 0.66, b = 0.960 and d = 0.6 as predicted for methane by the analytical model by Kolla et. al. The value for b is taken to be 1.6*d for methane/air flames with equivalence ratio of 1, and it is mentioned in [6] that although it (though specifically the K_C*/τ ratio, see Ch. 2.3) has yet to be calculated, other fuels should have values in roughly the same region. b is also the only of the three equation parameters which is expected to need adjustment for different equivalence ratios.

In fig. 21, pressure data from both the pressure transducers in the engine are displayed. Prior to ignition, there is a systematic discrepancy of about 10.000-20.000 Pa. It is not likely that pressure differences in the gas would be spatially static, so the discrepancy can be taken as a rough indication of the uncertainty in calibration of the experimental system. Minor semi-static pressure differences could be explained by the systematic structure of the gas flow in the cylinder, but the symmetrical setup makes this explanation unlikely.

The turbulent flame propagation model was also tested against experimental data with Φ = 0.77, 0.86, 1.20 and 1.28. The pressure traces for each equivalence ratio refer to individual cycles, whereas the temperature data given was cycle-averaged. Maximum and minimum values for temperature were also given, defining a certain span within which the initial temperature of the model was adjusted. Due to the stochastic nature of the early flame kernel development, the timing of the start of combustion (θ_0) was also adjusted in each individual case. The parameter b in eq. 26 is thought to be linearly dependent on Φ, and an attempt was made to pinpoint this relationship. All other parameters in the model (including the turbulence velocity u') remained unchanged. Fig. 22 – 25 display the

pressure output for the four cases.

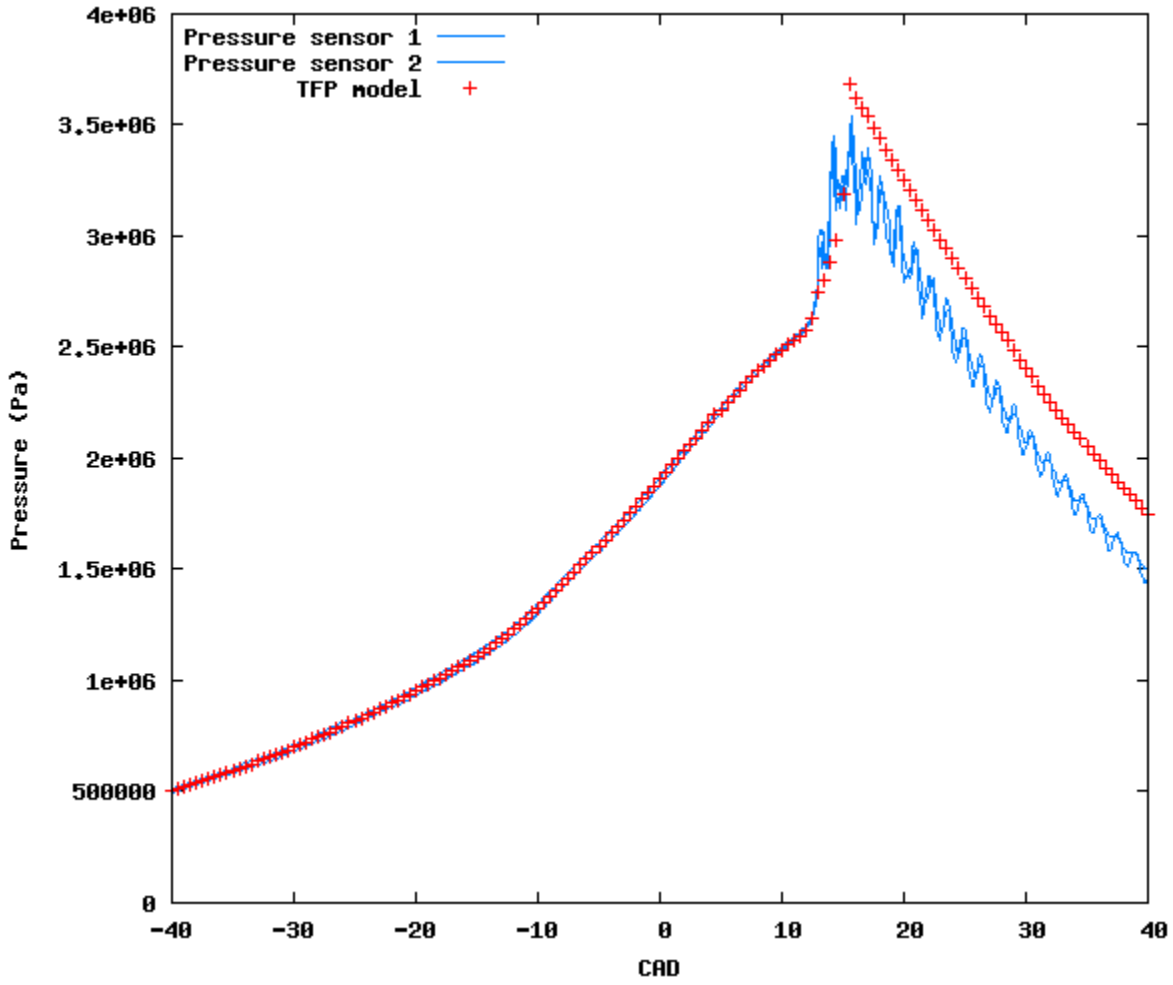

Fig. 22 – Pressure traces for TFP model and experimental data. Φ = 0.77, b = 0.802

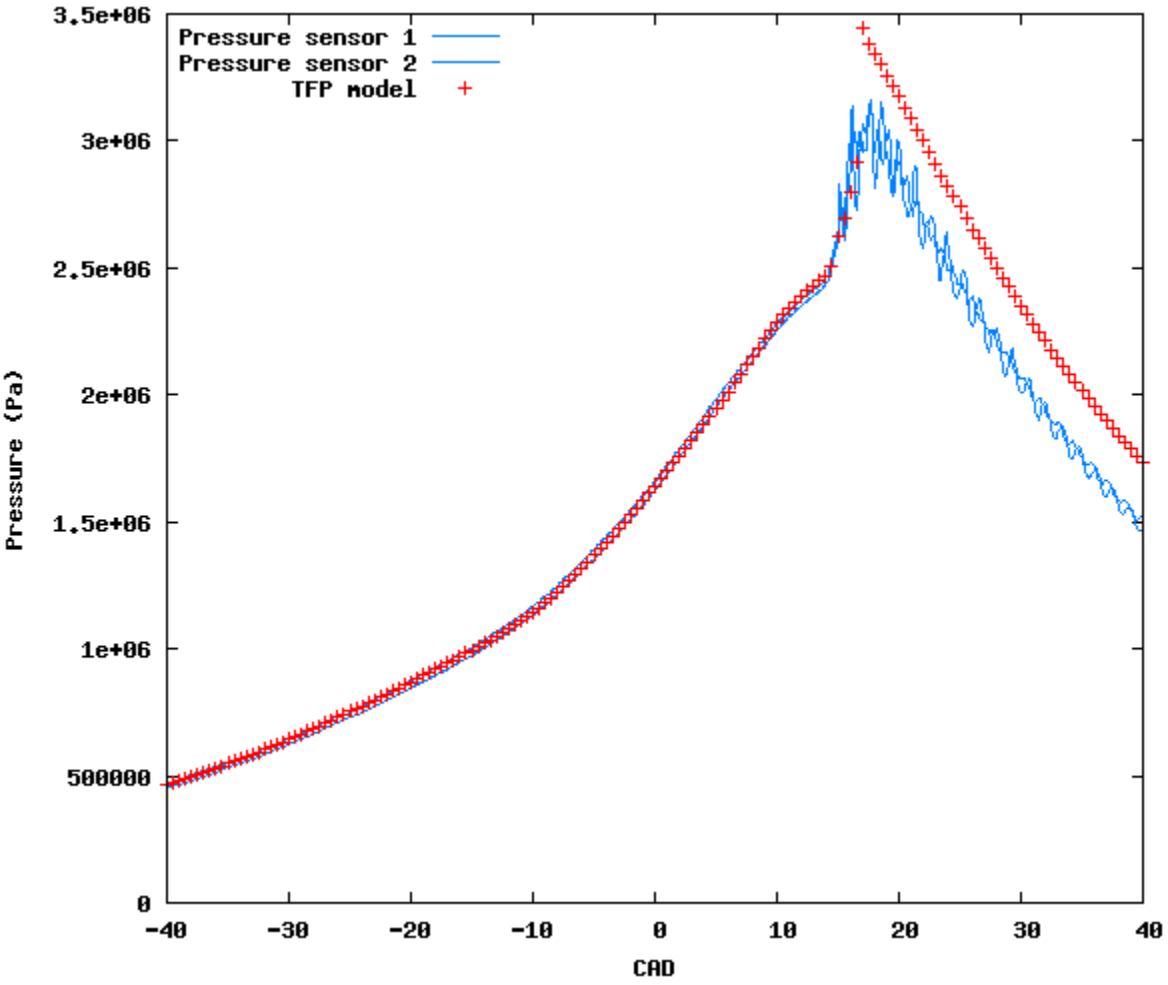

Fig. 23 – Pressure traces for TFP model and experimental data. Φ = 0.86, b = 0.803

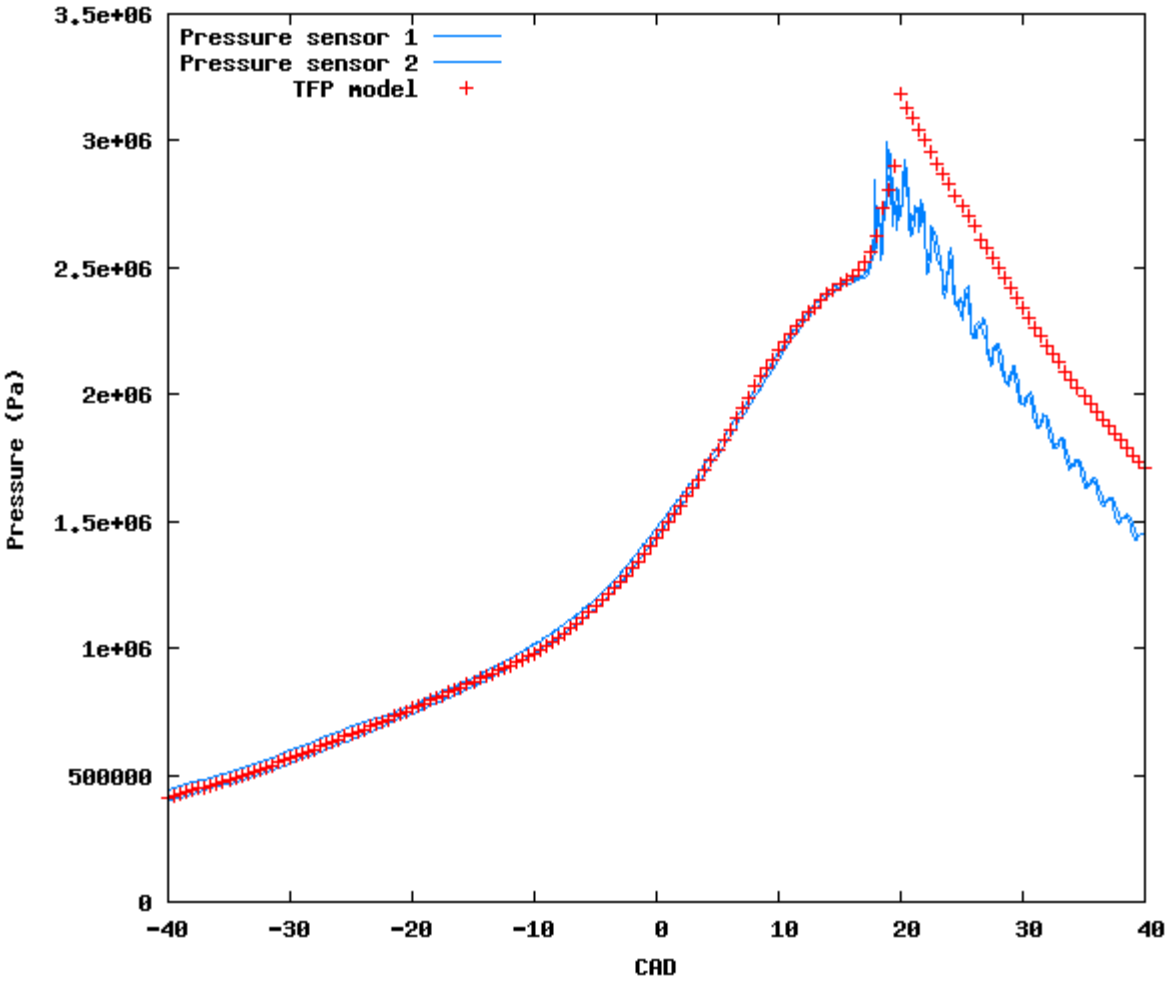

Fig. 24 – Pressure traces for TFP model and experimental data. Φ = 1.20, b = 0.808

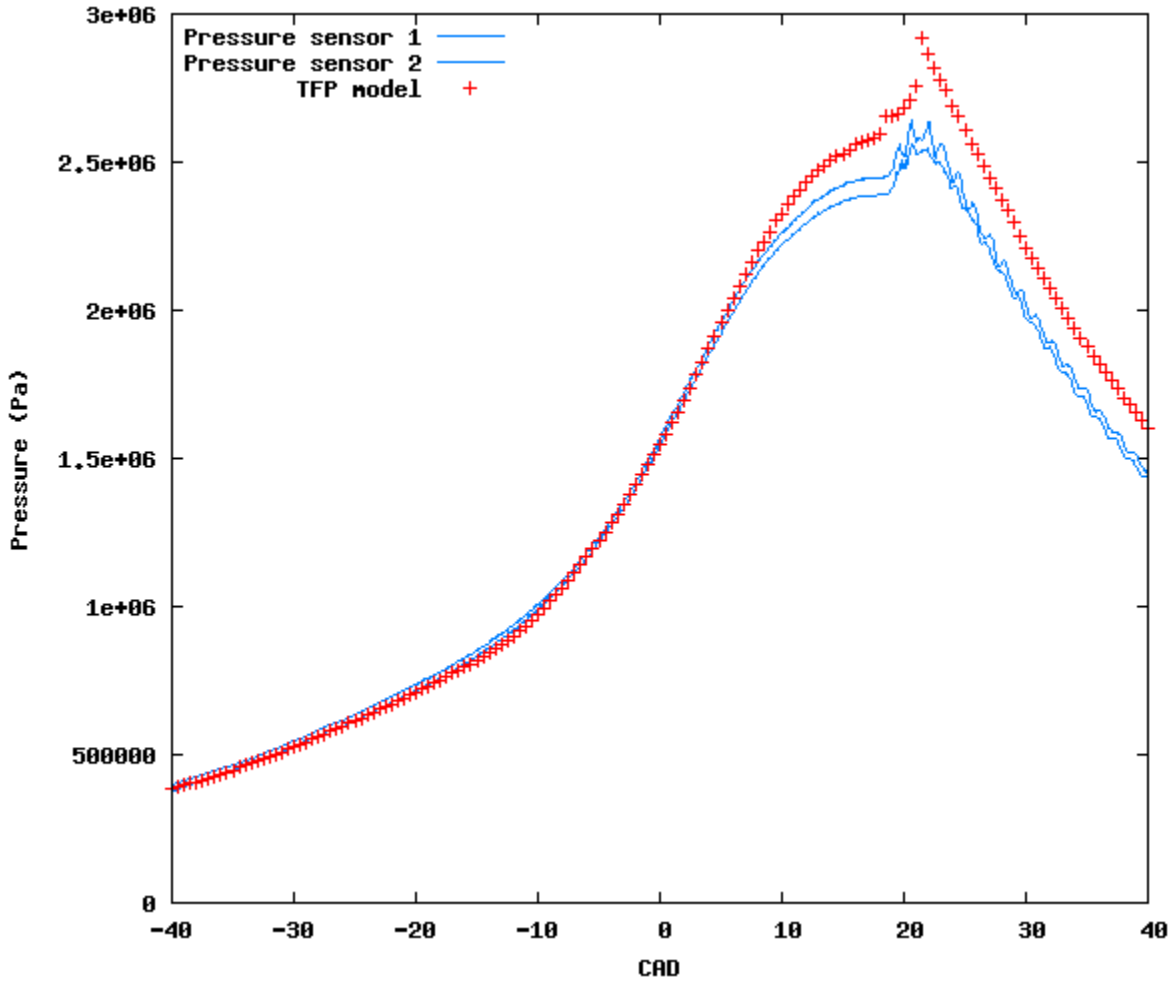

Fig. 25 – Pressure traces for TFP model and experimental data. Φ = 1.28, b = 0.810

Fig. 26 shows the required values for the parameter *b* as a function of the equivalence ratio. Compared to the K_C^*/τ-dependency for methane reported in [6] (of which *b* should be linearly dependent), the variations for iso-octane is smaller. The effects of these variations on the flame propagation speed (see Ch. 6.1) is insignificant compared to other factors like ignition timing and amount of fuel mass. In order to precisely examine the variations in *b* for different Φ, more exact data would be needed.

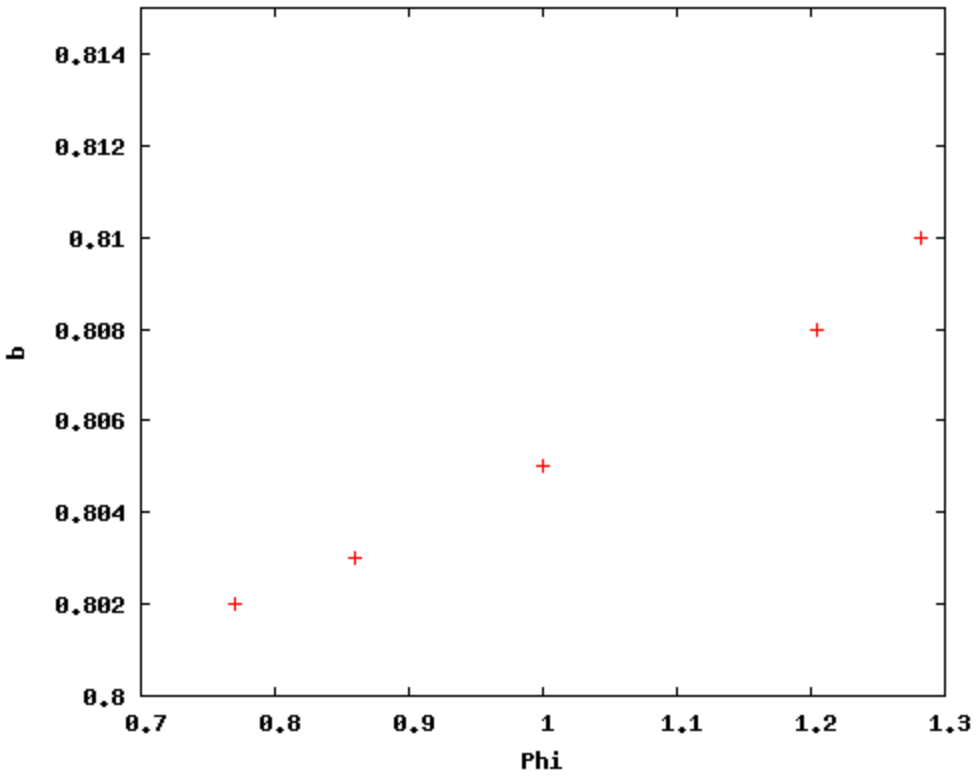

Fig. 26 – Fitted values for b at different equivalence ratios

It should also be noted that the model could not be made to produce satisfying results for Φ = 1.28 without modifying other parameters than those previously mentioned. This could be attributed to the cycle-resolution of the experimental data, but could also indicate a flaw in the generalizations and assumptions made for this particular case (see above). Another possible explanation, and perhaps the most likely one, is that the fitting turbulence velocity of 0.625 m/s (which was selected using the Φ = 1.00 case) contains compensations for geometric effects, such as an incorrectly calculated piston position. The relationship between the turbulent flame propagation speed and the equivalence ratio might then not follow the linear behaviour which was expected.

It was shown that the Monte Carlo model can be manipulated to simulate cases which do not fulfill the preconditions it was written for, with results at least as accurate as those achieved with a fitted Wiebe function. Furthermore, although it is possible that

generalizations affect the predictive capabilities of the model, one can expect that some predictive capabilities are conserved.

Table 2 contains the relevant engine paramers for the case.

Engine speed	1200 RPM
Displaced volume	745.5 cm^3
Bore / Stroke / Rod	96 / 103 / 158 mm
Compression ratio	8.22
Wall temperature	450 K

Table 2

6.3.2 2.0 l engine

Further validation of the model was made using experimental data from a 4 cylinder 2.0 l engine. Pressure traces were provided for each of the four cylinders, averaged over a number of cycles, see fig. 27. Further data were also provided based on previous simulations. Of the four cylinders, the one marked as “Cyl. 1” in fig. 27 was selected for validation.

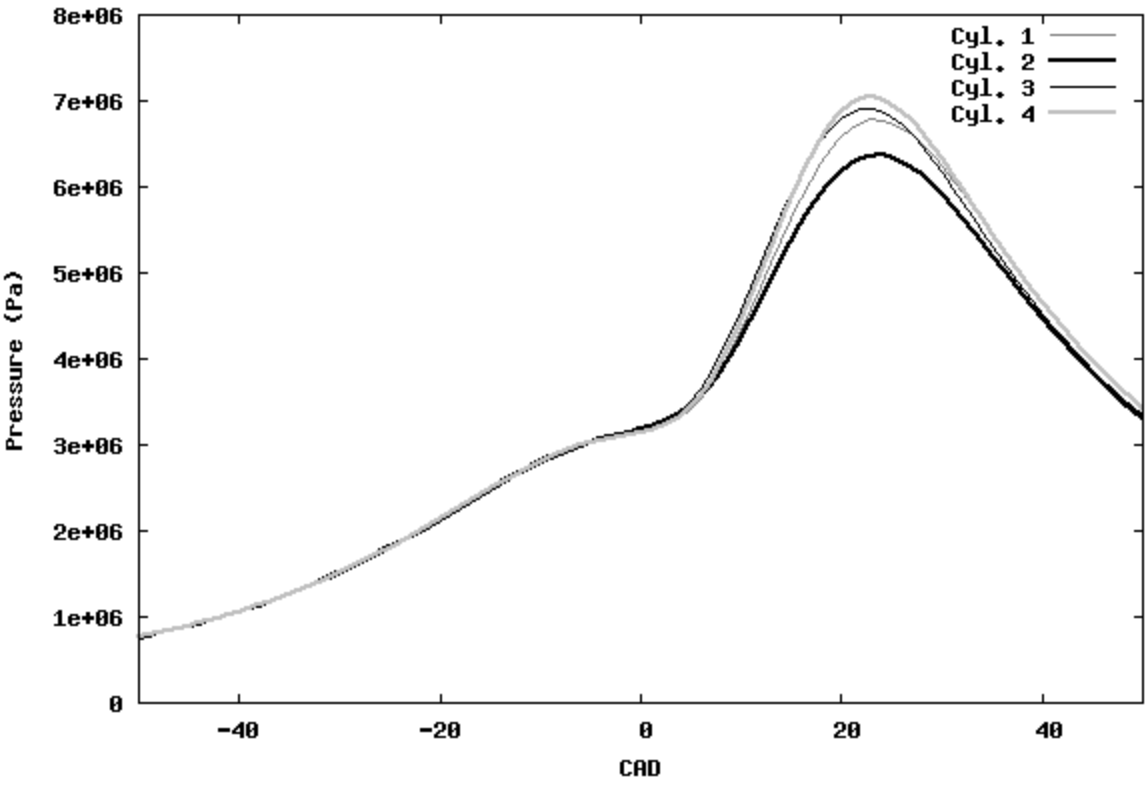

Fig. 27 – Pressure traces, 2.0 l engine

The geometry input was based on given measurements combined with a number of photos of the cylinder head and the piston. Detailed drawings were not available but the input profile created is thought to have a maximum deviation of 2 mm from the experimental setup. Simulations were performed using a cylinder with a flat piston top and one with a bowl of 3 mm maximum depth (according to descriptions provided with the experimental data). For a fixed clearance volume of 58.38 cm^3, this corresponds to a decrease in the minimum clearance between the piston and the squish areas from 2.65 mm to 1.51 mm, as illustrated below in Fig. 29.

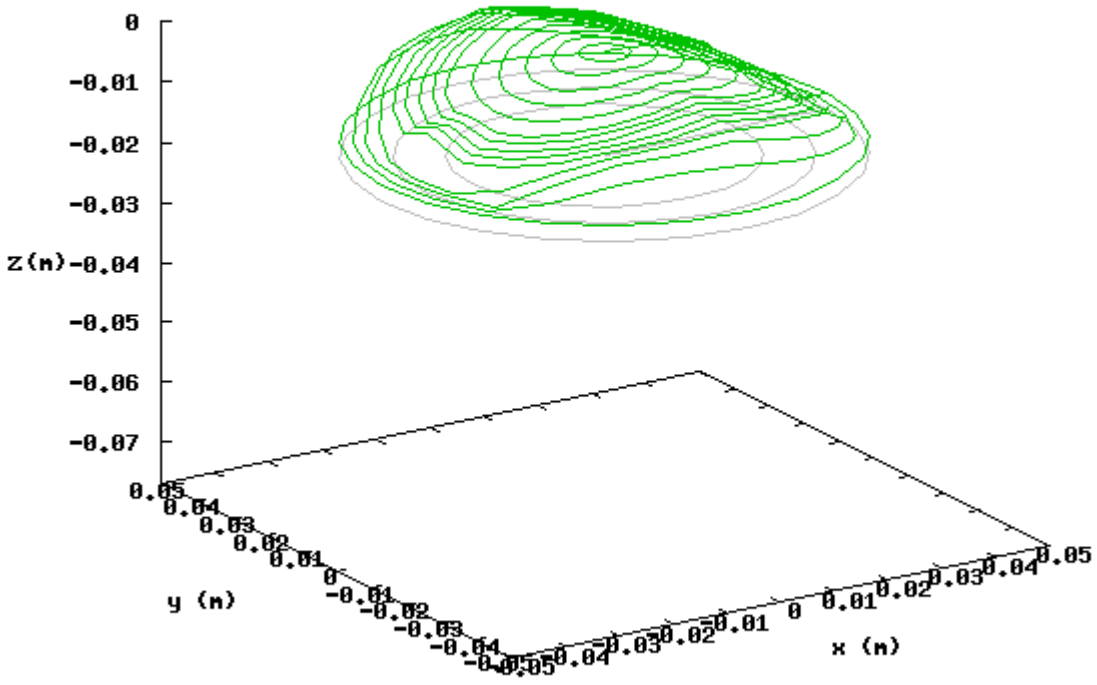

Fig. 28 – Cylinder profile and piston position at TDC without piston bowl

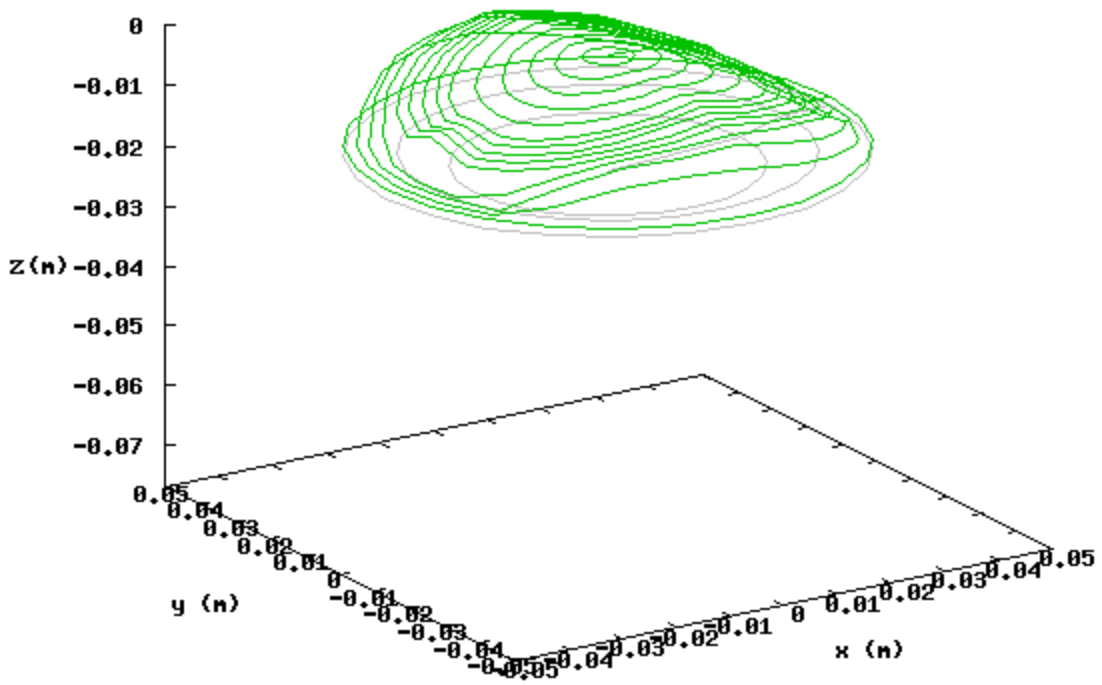

Fig. 29 – Cylinder profile and piston position at TDC with piston bowl (note the difference in clearance between the piston and the squish areas)

For the piston geometry with and without the piston bowl, a suitable ignition time was found together with a suitable τ-value. Other values were taken as defaults and the integral length scale was approximated to half the cylinder bore. For the case with the piston bowl, the fitting u' was 3.42 m/s and for the case without the bowl it was 3.50 m/s. The ignition timing was kept the same for both cases at -10.5 CAD BTDC, and in order to achieve a good fit the spark plug position was adjusted to 5.5 mm from the cylinder centre (as opposed to an estimated 3 mm provided with the setup data). A comparison between the resulting pressure traces is provided in Fig. 30 and 31, together with the pressure trace from cylinder 1 in the experimental setup.

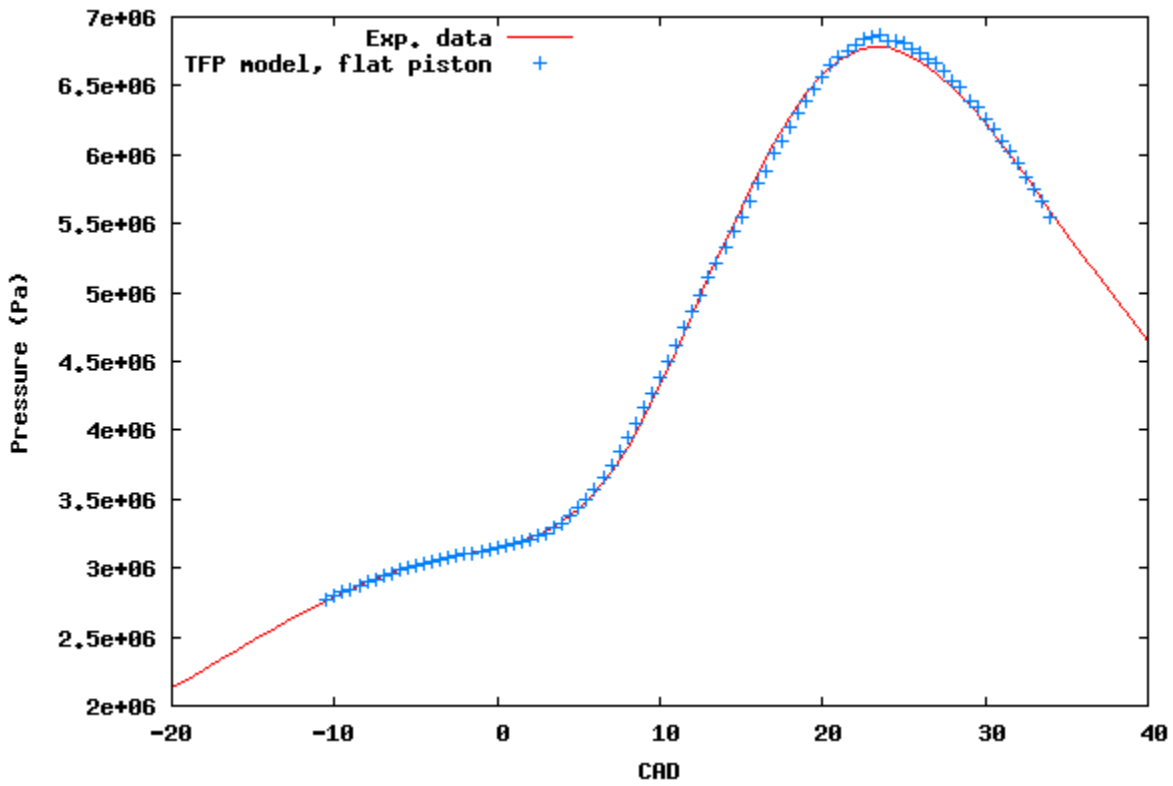

Fig. 30 – Pressure trace without piston bowl compared to exp. data

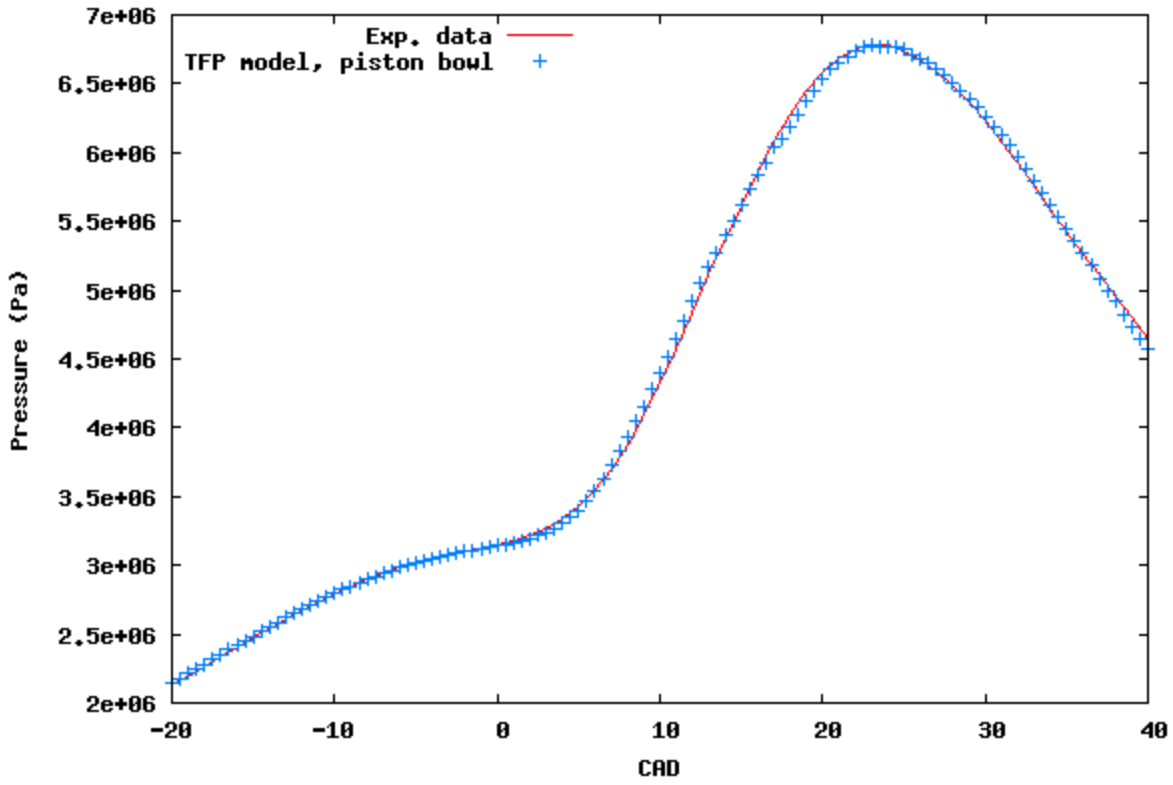

Fig. 31 – Pressure traces with piston bowl compared to exp. data

What is important to notice is the qualitative difference in behaviour based on a change in the scale of 1 mm in the geometry input. Having a geometric dependency of that scale is very promising for possible applications of the model. However, as mentioned above, the geometry input itself for this experiment was only available with a precision of approximately 2 mm. This might be one plausible explanation as to why the spark plug offset needed adjustment. Another explanation is that the flow field in the cylinder could have given rise to a translational movement of the flame sphere. Had the flame shape been significantly distorted by the flow field (with an inaccuracy greater than that in the geometry), then the qualitative behaviour of the model should be incorrect, but a translational movement of 1 m/s would be enough to yield similar results as to having a spark plug offset 2.5 mm too high.

A second concern which might affect the model behaviour would be the lack of a wall

quenching model in the later stages of combustion. When the amount of unburned gas reaches 5-10% of its original amount, a significant portion of that gas will be within a few mm of the cylinder walls, where wall quenching takes place. If the wall quenching phenomenon has a non-negligible effect, then the model output should burn the last portion of the fuel slightly too fast, resulting in a premature termination of the flame propagation phase. Fig. 32 and 33 show the pressure trace and the MFB curve for CAD 0 to 45 ATDC, and suggests that the combustion process of the final unburned gas should have been more extended. Another possible interpretation is that the model was fitted to a system with a slightly incorrect fuel/air equivalence ratio.

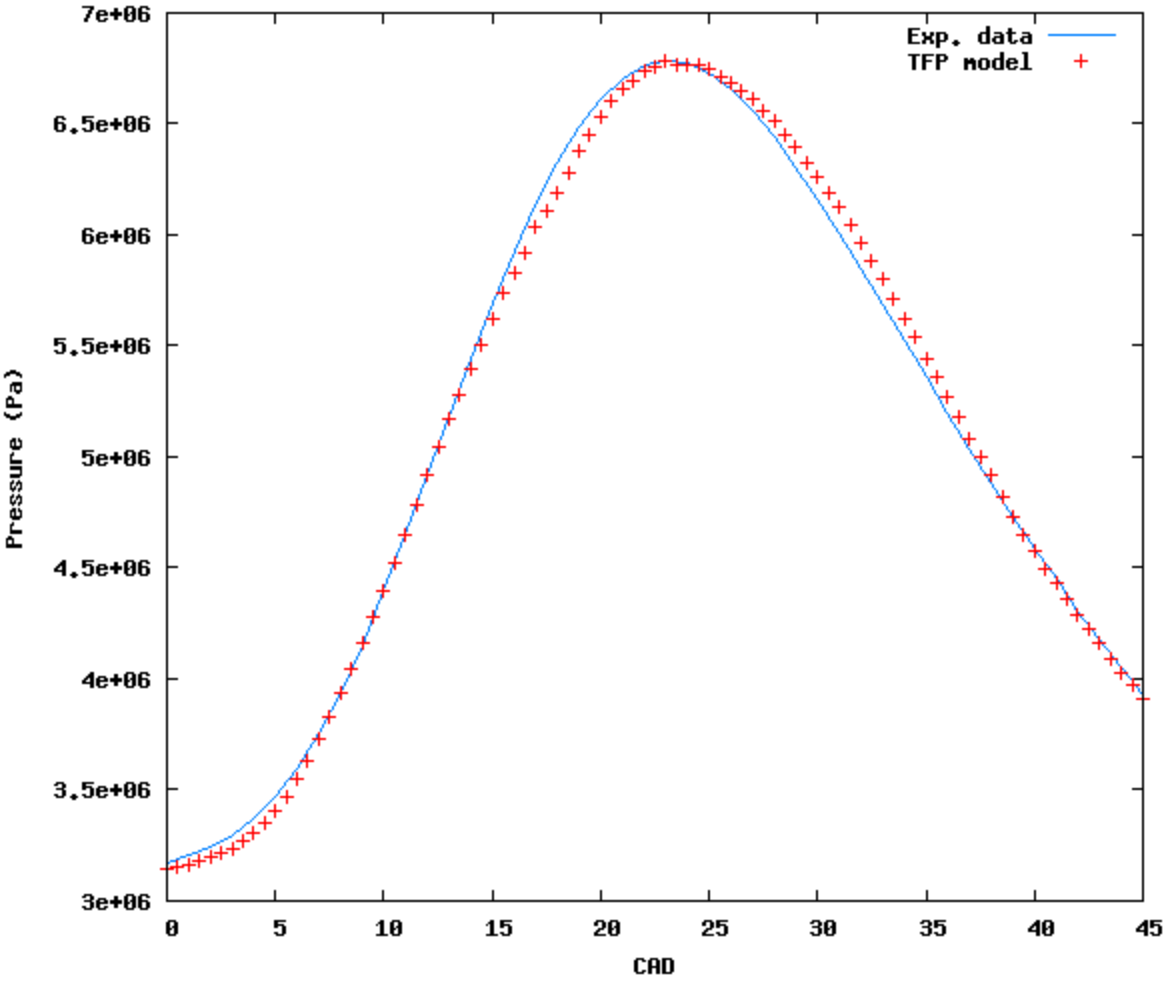

Fig. 32 – Pressure trace and TFP-SRM model (with piston bowl) and pressure trace for exp. data.

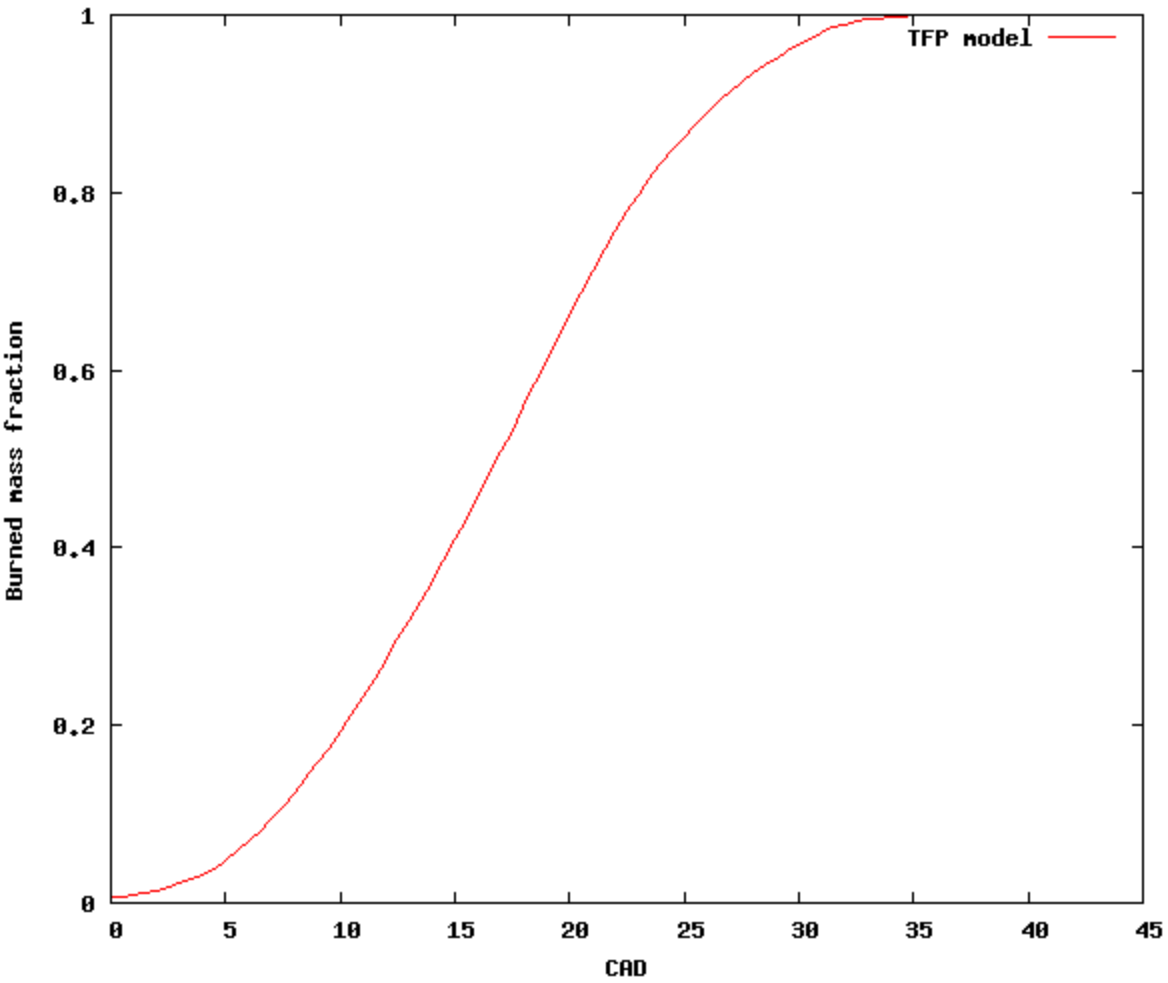

Fig. 33 – Burned mass fraction for TFP-SRM model

7. Conclusions

A model was developed for calculating turbulent flame speed using user-defined turbulence parameters and a laminar flame speed library. Assuming a spherical flame propagation, Monte Carlo geometry calculations were used to describe the combustion process and its geometry dependency. The model was integrated with an already existing SRM code, potentially replacing the non-predictive Wiebe function previously used in the SRM code and creating a possibility to do time-efficient geometry studies in an otherwise zero dimensional engine simulation code.

Validation confirmed that the model is capable of producing good results, and capable of modelling geometrical effects on a scale of 1-2 mm. The Monte Carlo model showed generally good correlation to a similar study performed by Poulos & Heywood [8], and the turbulence model appears to have a dependency of τ coherent with the one of the mixing model in the SRM.

Judging by the validation, the initial assumptions seemed acceptable. τ can be approximated as invariant during the combustion phase without much loss of precision, and the flame shape can be described as spherically expanding. The validation suggests that implementation of a wall quenching model could improve the results, but that satisfying results can be achieved even without such a model.

8. Future work

The Monte Carlo model was written so that it would be capable of calculating the volume of a near-wall layer for each zone, based on the flame shape and a user defined layer thickness. One could create a wall quenching algorithm as specified in ch. 4. Preferably, such an algorithm would be validated against experimental data for identical engines but with varying wall temperature. Together with a calculation of crevice volumes, this would offer a more correct calculation of the final pressure after combustion, particularly in cases with autoignition.

Parallelisation of the Monte Carlo algorithm would significantly decrease calculation times, building further on one of the strengths of the SRM code. One might also revise the algorithm to decrease the required number of Monte Carlo points with conserved precision.

Predictive calculations of the turbulent mixing time τ could be performed, possibly by describing a spectrum of kinetic energy per length scale, initialized by the fuel intake and

modified in each time step by dissipation and the piston movement. Judging by the sensitivity study in ch. 5, one should be able to fit a pressure trace with a precision in the region of 2 CAD and with an uncertainty in the maximum pressure of about 5-10%. For precision comparable to that of a fitted Wiebe-curve however, the model would probably still be dependent on user tweaking.

Finally, the model would benefit from a thorough study of the impact of the flow field in the cylinder, to set up limits for when the assumption of a spherically propagating flame is valid.

References

[1] Tunér, M. *Stochastic Reactor Models for Engine Simulations*. Doctoral Thesis, Division of Combustion Physics, LTH/Lund University 2008.

[2] Samuelsson, K. *Development and Validation of a Fuel Injection Model for the SRM Code.* MSc thesis, Department of Combustion Physics, Lund University, 2004.

[3] Peters, N. *Turbulent Combustion*. p 15ff. Cambridge University Press, 2000.

[4] Peters, N. *Turbulent Combustion*. p 122f. Cambridge University Press, 2000.

[5] Nilsson, P. and Bai, X.S. *Effects of Flame Stretch and Wrinkling on Co Formation in Turbulent Premixed Combustion*, Proceedings of the Combustion Institute, 2002, Volume 29.

[6] Kolla, H., Rogerson, J.W., Chakraborty, N. and Swaminathan, N. *Scalar Dissipation Rate Modeling and its Validation*, Combustion Science and Technology, 2009, 181:3, 518-535.

[7] Kolla, H., Rogerson, J.W. and Swaminathan, N. *Validation of a Turbulent Flame Speed Model across Combustion Regimes*, Combustion Science and Technology, 2010, 182:3, 284-308

[8] Poulos, S.G. and Heywood, J.B., *The Effect of Chamber Geometry on Spark-Ignition Engine Combustion*, 1983, SAE paper 830838, SAE Trans. vol. 92